EUROPEAN ORGANIZATION FOR NUCLEAR RESEARCH

CERN-EP/82-77
15 June 1982

EXPERIMENTAL STUDY OF OPPOSITE-SIGN DIMUONS PRODUCED IN NEUTRINO AND ANTINEUTRINO INTERACTIONS

H. Abramowicz*, J.G.H. de Groot, J. Knobloch, J. May, P. Palazzi, A. Para*,
F. Ranjard, J. Rothberg**, W. von Rüden, W.D. Schlatter, J. Steinberger,
H. Taureg, H. Wahl and J. Wotschack
CERN, Geneva, Switzerland

F. Eisele, H.P. Klasen, K. Kleinknecht, H. Lierl, B. Pszola,
B. Renk and H.J. Willutzki
Institut für Physik der Universität Dortmund, Dortmund, Germany

F. Dydak, T. Flottmann, C. Geweniger, J. Królikowski* and K. Tittel
Institut für Hochenergiephysik der Universität Heidelberg, Heidelberg, Germany

C. Guyot, J.P. Merlo, P. Perez, B. Peyaud, J. Rander, J.P. Schuller and R. Turlay
D.Ph.P.E., CEN-Saclay, France

J.T. He, T.Z. Ruan and W.M. Wu
Institute of High Energy Physics, Beijing, China

(Submitted to Zeitschrift für Physik)

---

*) On leave from the Institute of Experimental Physics, Warsaw University, Warsaw, Poland.
**) On leave from the University of Washington, Seattle, USA.

ABSTRACT

A large sample of opposite-sign dimuons, produced by the interaction of neutrinos and antineutrinos in iron, is analysed. The data agree very well with the hypothesis that the extra muon is the product of charm decay. They yield information on the strength and space-time structure of the charm-producing weak current. The strange-sea structure function $xs(x)$ is determined. The difference between neutrino and antineutrino dimuon production is analysed to provide a value of the Kobayashi-Maskawa weak mixing angle θ_2.

1. INTRODUCTION

After the first observation of opposite-sign dimuon events in muon neutrino interactions [1], several experiments using electronic detectors [2,3], as well as bubble chambers [4-6] have confirmed the hypothesis that single charm production and decay is the origin of opposite-sign dimuon events. In the quark parton model the charm-producing processes are expected to be the following:

$$\nu + d \rightarrow \mu^- + c$$

$$\nu + s \rightarrow \mu^- + c$$

$$\bar{\nu} + \bar{d} \rightarrow \mu^+ + \bar{c}$$

$$\bar{\nu} + \bar{s} \rightarrow \mu^+ + \bar{c} \ .$$

The second muon, of opposite charge, is the result of the semileptonic decay of the charmed particle:

$$c \rightarrow s + \mu^+ + \nu_\mu$$

$$\bar{c} \rightarrow s + \mu^- + \bar{\nu}_\mu \ .$$

These earlier experiments have also shown that new heavy particles, quarks, or leptons, can be excluded as a major source of dimuon events at present neutrino energies [2-7]. The new experiment that we describe here involves the reconstruction of a large sample of dimuon events from extended exposures in wide-band and narrow-band neutrino and antineutrino beams at the CERN SPS with the CDHS (CERN-Dortmund-Heidelberg-Saclay) detector [8]. The results are based on 10,381 neutrino and 3,513 antineutrino opposite-sign dimuon events from wide-band beams (WBBs) and 660 neutrino and 171 antineutrino events from narrow-band beams (NBBs). This is to be compared with 257 neutrino events and 58 antineutrino events in the previous publication [3]. The large increase in statistics permits a more thorough check of the charm hypothesis and allows the study of the V - A structure of the charm-producing current as well as the determination of the Kobayashi-Maskawa angle θ_2 [9], the measurement of the structure function of the strange sea, and the charm fragmentation function.

In the next section we describe the data reduction. In Section 3 we present the raw data sample. Section 4 outlines the theoretical formalism and Section 5 describes the Monte Carlo simulation. The results of the analysis of the data are presented in Sections 6-11.

2. EXPOSURES AND DATA REDUCTION

2.1 Beams

The neutrino and antineutrino WBBs were produced by protons of 350 and 400 GeV energy on a Be target followed by 300 m of decay space. The total intensities on target were respectively 5.2×10^{18} and 4.0×10^{18} protons. The horn and reflector focusing used for the WBB leads to neutrino spectra peaked around 20 GeV. The contamination of antineutrinos in the neutrino beam is small (less than 1%); however the contamination of neutrinos in the antineutrino beam is substantial and becomes dominant above 150 GeV. These characteristics are shown in Fig. 1. The neutrino and antineutrino beam spectra as well as background in the WBBs were obtained from the analysis of single-muon events of appropriate muon charge. Although lower in statistics, data from NBB exposures are interesting because of different beam characteristics: the wrong-sign background is negligible, there is a correlation between neutrino energy and radial position of the interaction vertex in the detector, and the shape of the energy spectrum is accurately known and it is flat [10].

2.2 Apparatus and trigger

The events were observed with the detector described previously [8]. In the WBB the multimuon trigger requires two or more hits in at least two of the three planes of four or more adjacent drift chambers. This requirement implies that each muon must have a minimum energy of 3.5 GeV. The capability of the readout system is such that up to four hits on the same drift wire can be detected if separated by at least 7 mm in space (140 ns in drift-time). In addition to the drift chamber requirement, a minimum of 7 GeV muonic or hadronic energy deposition in the calorimeter was demanded. In the NBB exposures no special trigger is required for dimuon events; they are included in the normal single-muon event trigger (deposition of

hadron energy of at least 3 GeV, or minimum ionizing particle in three modules). The dimuons are selected later by software, using the same criteria as those for the WBB dimuons.

2.3 Event selection

Initially all NBB events, and a subsample of 2,000 neutrino WBB events were scanned and measured by hand using an interactive pattern recognition and track-fitting program. These interactively-measured events were used to determine the efficiency and to evaluate the biases of the off-line reconstruction program with which subsequently the entire sample was processed. The off-line program accepts events only if both muons traverse at least five chambers and fulfil the following requirements:

- One μ^- and one μ^+ are found and successfully fitted.
- The fit of each track has to start at least in the third drift chamber downstream from the vertex.
- The separation ΔR of the two tracks at the vertex is less than 15 cm. (The mean value of the ΔR distribution is 7.5 cm.)

After these cuts 80 ± 5% of those $\mu^+\mu^-$ events survived where both muons traverse five chambers. The comparison with the sample of hand-measured events shows that no significant shifts or biases on the measured quantities are introduced by the off-line reconstruction program.

Dimuon events are accepted for the final analysis if they satisfy the following selection criteria:

- The event vertex is required to be within the first 14 of the 19 modules.
- The vertex has to be within a circle of 1.6 m radius around the centre of the toroids.
- Events near the centre of the apparatus are excluded (cut 51 cm wide, 26 cm high).
- Both muon momenta have to be larger than 5 GeV/c.
- The total visible energy E_{vis} (as defined in Section 3) is required to be at least 20 GeV.

A total of 10,381 events in the neutrino WBB and 3,513 events in the antineutrino WBB, and 660 and 171 respectively in the NBB survive these cuts.

2.4 Separation of neutrino- and antineutrino-induced events in antineutrino exposure

In the neutrino WBB the contamination of antineutrinos is sufficiently low to be neglected in the analysis. In the antineutrino WBB, however, one third of the observed dimuon events is due to the neutrino background in the beam. In this case the antineutrino-induced dimuon events can be extracted with acceptable purity on the basis of the transverse muon momenta p_T^+ and p_T^- with respect to the hadron shower direction. The latter is defined as the direction which balances the negative muon momentum in the neutrino beam and the positive muon momentum in the antineutrino beam. The scatter plot p_T^+ versus p_T^- for the events from the neutrino WBB is shown in Fig. 2a. The opposite-sign transverse momentum p_T^+ is in general limited. Figure 2b shows the same scatter plot for the antineutrino WBB events. The bulk of the large p_T^- events in this plot must be attributed to the neutrino contamination. Antineutrino-induced events have been selected by the requirement $p_T^+ > p_T^-$. The correction for migration of neutrino events into the "$\bar{\nu}$ region" and for the loss of $\bar{\nu}$ events due to this selection has been evaluated using a Monte Carlo program. The net correction of 6 ± 1% is almost independent of energy. The procedure is verified with data taken in the relatively pure neutrino beam. The systematic uncertainties are small compared with the statistical errors of the sample of antineutrino-induced events. Table 1 gives the decomposition of the dimuon events from the antineutrino WBB as a result of this separation procedure.

2.5 Background from π or K decay

There is a background due to non-charmed muonic decays, chiefly π and K decay. Details of the Monte Carlo calculations of this background are given elsewhere [11]. The average contamination due to π and K decay is 13% in neutrino, and 6% in antineutrino interactions. The variation with respect to the neutrino energy is small as seen in Fig. 3. Throughout this analysis these backgrounds have been subtracted from the experimental samples.

3. RAW DATA

We define here the variables used in the following analysis. The neutrino direction is assumed to be parallel to the axis of the detector.

p_{μ_1} = momentum of the muon carrying the same lepton number as the incident neutrino. This is the "leading muon", i.e. μ^- for neutrino-induced events and μ^+ for antineutrino-induced events.

p_{μ_2} = momentum of the "second" muon

E_{sho} = hadron shower energy

$E_{had} = E_{sho} + p_{\mu_2}$

$E_{vis} = E_{sho} + p_{\mu_2} + p_{\mu_1}$

E_ν = energy of incident neutrino

$\nu = E_\nu - p_{\mu_1}$ = energy transfer

θ = angle between $\vec{p}_{\mu_1}$ and the neutrino direction

$Q^2 = 4\, E_{vis}\, p_{\mu_1} \sin^2 \theta/2$

$x = 4\, E_\nu\, p_{\mu_1} \sin^2 (\theta/2)/(2M_N \cdot \nu)$

$x_{vis} = Q^2/(2M_N \cdot E_{had})$

M_N = mass of the nucleon

$y = \nu/E_\nu$

$y_{vis} = E_{had}/E_{vis}$

Φ = angle between the projections of $\vec{p}_{\mu_1}$ and $\vec{p}_{\mu_2}$ on a plane perpendicular to the neutrino direction

$\vec{p}_{had} = \vec{p}_\nu - \vec{p}_{\mu_1}$ = hadron shower momentum

p_T = transverse momentum of muon (either leading muon or second muon) relative to $\vec{p}_{had}$

$W_{vis} = (2M_N \cdot E_{had} + M_N^2 - Q^2)^{1/2}$

m_{12} = invariant mass of the muon pair = $\left[(E_1 + E_2)^2 - (\vec{p}_{\mu_1} + \vec{p}_{\mu_2})^2\right]^{1/2}$

α = momentum asymmetry = $(p_{\mu_1} - p_{\mu_2})/(p_{\mu_1} + p_{\mu_2})$

E_D = energy of D meson

E_c = energy of primary charmed quark

$z = E_D/E_c$

$z_L = p_{\mu_2}/(p_{\mu_2} + E_{sho})$.

Distributions of the data are presented in Figs. 4a, b, c, and d for the neutrino and antineutrino samples. Some general comments can be made:

i) The momentum of the second muon p_{μ_2} is smaller than that of the leading muon p_{μ_1}.

ii) The p_T distribution, as well as the Φ distribution which is peaked at 180°, shows that the second muon is associated with the hadronic shower.

iii) The shape of the y_{vis} distribution is biased by the minimum momentum requirement for the muons. The cut-off on p_{μ_2} and consequently on E_{had} depopulates the small y_{vis} region, whereas the cut-off on p_{μ_1} depopulates the large y_{vis} region. The Monte Carlo curves shown in Fig. 4 correspond to a flat generated y distribution.

iv) The x_{vis} distributions are narrower in the antineutrino data than in the neutrino data. These in turn are narrower than the structure functions $F_2(x)$ and $xF_3(x)$ of single-muon reactions.

v) The W_{vis} and m_{12} mass plots do not show significant structure.

The dimuon event numbers are presented in Table 2. The single-muon event numbers also shown in the table are based on a normalized subsample of the data. In this table, the visible energy for single-muon events equals the neutrino energy, while the visible energy for dimuon events is smaller because of the energy lost by an escaping neutrino from the semileptonic decay producing the second muon. In order to compare dimuon and single-muon event rates, in bins of true neutrino energy, a correction must be applied to the visible energy (see Section 6).

4. THEORETICAL FRAME FOR THE ANALYSIS

A model of charm-producing weak currents was proposed by Glashow, Iliopoulos and Maiani (GIM) [12], even before charm was experimentally discovered. The GIM current has the following structure:

$$J_\mu^{GIM} = (\bar{u},\bar{c})\ \gamma_\mu(1+\gamma_5)\begin{pmatrix} \cos\theta_c & \sin\theta_c \\ -\sin\theta_c & \cos\theta_c \end{pmatrix}\begin{pmatrix} d \\ s \end{pmatrix} + \text{h.c.}\ ,$$

where θ_c is the Cabibbo angle.

Charm is produced with amplitude $\sin\theta_c$ from d quarks, and with amplitude $\cos\theta_c$ from s quarks. We now know that there are not four, but at least five quarks: the extension to three flavour pairs is due to Kobayashi and Maskawa (KM) [9] and involves three mixing angles and one phase in place of the single Cabibbo angle:

$$J_\mu^{KM} = (\bar{u},\bar{c},\bar{t})\ \gamma_\mu(1+\gamma_5)\,\mathcal{U}\begin{pmatrix} d \\ s \\ b \end{pmatrix} + \text{h.c.}$$

where $\mathcal{U}$ is the 3×3 KM matrix.

The important contributions to charm production are the processes:

$$\nu + d \to \mu^- + c$$

$$\nu + s \to \mu^- + c\ ,$$

and their charge conjugates. The conversion of a bottom quark to a charm quark can be expected to be negligible at our energies because of the high threshold and the smallness of the bottom structure function. The conversion of a charm quark to either d or s, with production of its associated (anti) charm quark can also be ignored because of the smallness of the charm structure function and our experimental biases, which make the detection of charm produced essentially at rest very inefficient.

If the charm-producing currents are left-handed, as the other known charged weak currents, then the cross-sections on isoscalar nuclei are

$$\frac{d\sigma^\nu}{dxdy} = \frac{G^2 M E_\nu x}{\pi}\left[U_{cd}^2\left[u(x) + d(x)\right] + |U_{cs}^2|2s(x)\right] \qquad (1)$$

and

$$\frac{d^2\sigma^{\bar{\nu}}}{dxdy} = \frac{G^2 M E_\nu x}{\pi}\left[U_{cd}^2\left[\bar{u}(x) + \bar{d}(x)\right] + |U_{cs}^2|2\bar{s}(x)\right]\ , \qquad (2)$$

where $u(x)$, $d(x)$, and $s(x)$ are the quark density distributions in the proton. We denote the integrals of the quark structure functions by $U = \int xu(x)\,dx$, $D = \int xd(x)\,dx$, $S = \int xs(x)\,dx$, and analogously for antiquarks. In the GIM [12] model $U_{cd} = \sin\theta_c$ and $U_{cs} = \cos\theta_c$. In the KM [9] notation $U_{cd} = \sin\theta_1 \cos\theta_2$ and $U_{cs} = \cos\theta_1 \cos\theta_2 \cos\theta_3 - \sin\theta_2 \sin\theta_3\, e^{i\delta}$.

At present only two of these angles are known with any confidence: $\sin\theta_1 = 0.228 \pm 0.011$ and $\cos\theta_3 = 0.96^{+0.04}_{-0.09}$ [13]. As we will see, neutrino charm-production experiments can contribute to the understanding of θ_2.

We note that in distinction to the usual (i.e. not charm-producing) cross-sections, the charm-producing cross-sections are uniform in y; the $(1-y)^2$ terms are absent because the interaction proceeds solely on quarks for neutrino collisions, and solely on antiquarks for antineutrino collisions. Right-handed weak charm-producing currents would be characterized by $(1-y)^2$ dependences, and this provides the possibility of an experimental test of the chirality of the charm-producing current.

The data must be corrected for the threshold effect due to the mass m_c for the charm quark, the so-called slow rescaling. To correct for this kinematical effect [14] the structure functions in Eqs. (1) and (2) should be replaced by functions of the variable $\xi = x + m_c^2/(2M_N\nu)$, $F(x) \to F(\xi)$ for $Q^2 \to \infty$, and the expressions multiplied by the factor $(1 - y + xy/\xi)$:

$$\frac{d^2\sigma^{\nu}}{dxdy} = \frac{G^2ME\xi}{\pi}\left(1 - y + \frac{xy}{\xi}\right)\left\{U_{cd}^2\left[d(\xi) + u(\xi)\right] + U_{cs}^2 2s(\xi)\right\} \qquad (3)$$

and

$$\frac{d^2\sigma^{\bar{\nu}}}{dxdy} = \frac{G^2ME\xi}{\pi}\left(1 - y + \frac{xy}{\xi}\right)\left\{U_{cd}^2\left[\bar{d}(\xi) + \bar{u}(\xi)\right] + U_{cs}^2 2\bar{s}(\xi)\right\} . \qquad (4)$$

We have set $m_c = 1.5$ GeV in the following.

5. MONTE CARLO SIMULATION OF CHARM PRODUCTION

The second muon, the one which is the product of charm decay, is the result of a complex process, including charm-quark fragmentation and charmed-particle decay. Comparison of our data with the hypothesis of charm production has been carried out with the help of a Monte Carlo simulation in which:

i) The y distribution is taken to be constant.

ii) The valence x distribution is $\sqrt{x}\,(1-x)^{3.5}$ and the sea x-distribution $(1-x)^7$.

iii) The production of charmed baryons is not considered. This is justified by the observation [19] that, for $E_\nu > 30$ GeV, out of twenty-six decays of charmed particles at most two are interpreted as Λ_c.

iv) The charm-quark fragmentation function is chosen to fit the experimental results, as discussed in Section 8.

v) The transverse momentum distribution of the charmed mesons with respect to the direction of the hadron shower is

$$\frac{dN}{dp_t^2} \propto \exp\left[-6(p_t^2 + M_D^2)^{1/2}\right],$$

to fit the experimental p_t distribution.

vi) The branching ratios for the decay modes $K^*\mu\nu$, $K\mu\nu$, and $\pi\mu\nu$ are taken to be 0.37/0.56/0.06 [15].

In every case the analysis has been performed with and without the assumption of slow rescaling (see Section 4).

6. MISSING ENERGY

If the interpretation of charm decay is correct, some of the energy of the incident neutrino is missing in the observed event because the neutrino emitted in the charm decay escapes detection. This can be studied in the NBB, because here the incident neutrino energy is related to the impact radius of the neutrino event in the detector, as can be seen in Fig. 5b for the single-muon events. The observed energy distributions agree well with the kinematic expectations. For dimuon events the observed energy distribution is shifted to lower energies (Fig. 5a) on the average by 12 ± 1%. This is in good agreement with the expectation of charm origin on the basis of a Monte Carlo calculation (Fig. 6). The average predicted energy loss is 12.3 ± 2%. The missing energy has already been demonstrated in an earlier publication [3], but the present result is more precise.

7. y DISTRIBUTIONS AND V - A STRUCTURE OF THE CHARM PRODUCING CURRENT

As discussed in Section 4, the neutrino and antineutrino y distributions for single-charm production are expected to be flat for left-handed, and of the form $(1-y)^2$ for right-handed currents.

As explained before the observed $d\sigma/dy$ distributions are seriously distorted by the minimum energy requirement for the two muons. The simulation of this bias, which is less severe at high than at low neutrino energy, depends on the choice of the charm-fragmentation function. In the analysis the experimentally observed distribution (see next section) was taken.

The solid curves in Fig. 7 are the expectations for purely left-handed currents. The dashed curves in Fig. 7 show the expected y_{vis} distributions for purely right-handed currents with the same fragmentation function. The good agreement with V - A shows that only a small admixture of V + A coupling can be accommodated by the data.

A parametrization of the form $d\sigma/dy \propto \beta(1-y)^2 + (1-\beta)$ gives the following upper limit on the parameter β at the 95% confidence level:

E_ν (GeV)	30–50	50–100	100–150	$\geq$ 150
β	$\leq$ 0.30	$\leq$ 0.10	$\leq$ 0.10	$\leq$ 0.34

For the combined data, and within the uncertainties of the fragmentation function, the limit $\beta < 0.07$ for the relative strength of the square of the right-handed current coupling constant can be deduced, at the 95% confidence level.

8. CHARM FRAGMENTATION

The fragmentation of heavy quarks into their appropriate heavy hadrons is expected to be harder than that of the light quarks (u, d, and s) into light hadrons [16]. It is expected that a charmed hadron coming from the fragmentation of a charm quark will carry most of the quark momentum. A first measurement of the charm fragmentation function D(z), i.e. the distribution in the charm fragmentation variable $z = E_D/E_c$ was done by studying the observed distribution in $z_L = p_{\mu_2}/(p_{\mu_2} + E_{sho})$, as shown in Fig. 8. It is obvious that the data require a hard fragmentation function. D(z) has been determined in a Monte Carlo fit to the two-dimensional distribution of dimuon data in z_L and $y_{had} = E_{had}/E_{vis}$, leaving D(z) as free parameters in 5 bins in z. The best fit to this distribution was obtained with the fragmentation function D(z) as shown in Fig. 9. It should be noted that the data points D(z) are correlated such that the detailed shape of D(z)

is not reliably obtained. For instance, the simple function $D(z) = \delta(z - 0.68)$ also gives an adequate fit to the data. On the other hand, the first moment of D(z) is well determined. It is $\langle D(z) \rangle = 0.68 \pm 0.05$, where the error is statistical. The systematic error from the following sources was estimated: uncertainties in (i) the π- or K-decay background calculation, (ii) the branching ratios of D mesons into K or K^* final states, (iii) the charm quark mass used in the slow rescaling correction. These effects contribute about equally to the total systematic error of 0.06. We therefore give the result including systematic error, $\langle z \rangle = 0.68 \pm 0.08$. This compares well with the theoretical values at our average Q^2 of 20 $(GeV/c)^2$ [16].

9. THE STRANGE-SEA STRUCTURE FUNCTION

The antineutrino dimuon production, in the GIM model, and also in the KM model if the mixing angles are not large, is dominated at the level of $\sim$ 90% by $xs(x)$. The remaining smaller contribution is due to the non-strange sea $x[\bar{u}(x) + \bar{d}(x)]$. The observed x distribution is experimentally indistinguishable from the $x[\bar{u}(x) + \bar{d}(x) + 2\bar{s}(x)]$ sea measured in single-muon production by antineutrinos at large y [10], so that the x distribution for antineutrino-induced dimuons in Fig. 10a is directly a measurement of the structure function of the strange sea $xs(x)$.

10. DIMUON TO SINGLE-MUON PRODUCTION RATIOS

Approximately 30% of the neutrino data and 60% of the antineutrino data were analysed also for the much more numerous single-muon events. Instead of dimuon cross-sections we give the ratios of dimuon to single-muon rates. This quantity is more directly obtained, and can be converted into absolute dimuon cross-sections on the basis of the single-muon absolute cross-sections [10]. Since the measured energy E_{vis} for the dimuon events, the sum of the two muon energies and the hadron energy, misses the outgoing neutrino energy (see Section 3), the measured energies are corrected by the energy-dependent factor shown in Fig. 6 to give the neutrino energy E_ν, at least on the average. All cross-section ratios given in the following are subject to a 10% scale error.

The raw ratios, corrected only for πK background, are shown in Figs. 11a and 12a. The acceptance corrections include reconstruction efficiencies, geometrical corrections (small), and the effect of the minimum muon-energy requirement. The dimuon acceptance -- the same for neutrino and antineutrino events -- is shown in Fig. 13 for two cases of the fragmentation function $D(z) = \delta(z - 0.68)$ as well as for another function $D(z)$ = constant, so that the effect of the fragmentation function may be judged. The acceptance-corrected results are shown in Figs. 11b and 12b. The solid error bars indicate the statistical errors only. The dotted error bars include the uncertainty of the fragmentation function. The ratio of neutrino to antineutrino $2\mu/1\mu$ production ratios ("double ratio") is shown in Fig. 14. In Fig. 15 our neutrino results are compared with bubble-chamber measurements [17,18] of $\mu^- e^+$ production. The bubble-chamber data are of particular interest because the positrons are detected even at quite low energy (0.3 GeV) and the result is therefore much less affected by uncertainties in $D(z)$. It is not possible to compare our results with other counter experiments because data corrected for acceptance and for missing energy are not available.

11. AMOUNT OF STRANGE SEA AND $\cos^2 \theta_2$

The amount of the strange sea and $\cos^2 \theta_2$ of the KM model can be deduced, subject to assumptions, from these results. Here we will find the momentum fraction of the strange sea, $S = \int_0^1 xs(x)\, dx$, or rather the quantity $S|U_{cs}^2|/U_{cd}^2$, from the shape of the x dependence of the neutrino dimuon production, and the quantity BU_{cd}^2 from the difference of the neutrino and antineutrino total cross-sections. Here B is the muonic branching ratio of the charmed particle. In the following analysis it is assumed that it is the same for neutrino- and antineutrino-produced charm. From these two quantities U_{cd}^2 and $|U_{cs}^2|S$ can be determined if B is known.

11.1 Determination of U_{cd}^2

From the neutrino and antineutrino dimuon to single-muon cross-section ratios, the quantity BU_{cd}^2 is determined as follows:

$$BU_{cd}^2 = \frac{\left(\sigma^{\nu}_{\mu^-\mu^+}/\sigma^{\nu}_{\mu^-}\right) - \left(R\sigma^{\bar{\nu}}_{\mu^+\mu^-}/\sigma^{\bar{\nu}}_{\mu^+}\right)}{1 - R} \frac{2}{3} . \qquad (5)$$

Here R is the ratio of antineutrino to neutrino total cross-sections, $R = \sigma^{\bar{\nu}}_{\mu^+}/\sigma^{\nu}_{\mu^-} =$ $= 0.48 \pm 0.02$ [10]. The dimuon to single-muon cross-section ratios, corrected for acceptance and slow rescaling, are shown in Figs. 16a and b. The results for $U_{cd}^2 B$ are given in Table 3. Within the statistical errors, the results are consistent with the average in the energy region $80 < E_\nu < 160$ GeV: $U_{cd}^2 B = (0.41 \pm 0.07) \times 10^{-2}$.

If slow rescaling were neglected the result would be $U_{cd}^2 B = (0.39 \pm 0.05) \times 10^{-2}$, which is very similar. A 10% increase (decrease) in the mass of the charm quark used in the slow rescaling correction increases (decreases) U_{cd}^2 by 2%. For the semileptonic branching ratio, a value of $B = (7.1 \pm 1.3)\%$ is obtained by using the following experimental results: in an emulsion experiment on neutrino interactions in a 350 GeV WBB [19], it is found that above a visible energy of 30 GeV chiefly D mesons are produced, specifically a mixture of $32 \pm 11\%$ D^+ and $68 \pm 11\%$ D^0 mesons. For this composition of D mesons, using the measured [14,20,21] average leptonic branching ratio for a 44%:56% mixture of D^+:D^0 in e^+e^- reactions -- $B' = (8.2 \pm 1.2)\%$ -- and the less precise separate semileptonic branching ratios for D^+ and D^0 [21] as constraints, the quoted value of B is obtained.

With this value $|U_{cd}| = 0.24 \pm 0.03$. In the GIM model [12] U_{cd} is just the sine of the Cabbibo angle, and our experimental result is in good agreement with the accepted value $\sin\theta_c = 0.230 \pm 0.003$ [22]. In the KM model [9], $U_{cd} =$ $= \sin\theta_1 \cos\theta_2$, where $\sin\theta_1 = 0.228 \pm 0.011$ [13]. We therefore find $\cos\theta_2 =$ $= 1.05 \pm 0.14$. A 10% variation of the leptonic branching ratio B induces a 5% shift on U_{cd}, and a *difference* of 10% between the leptonic branching ratios of D^0 and $\overline{D^0}$ causes a 7.5% variation in U_{cd}. This, to our knowledge, is the first measurement of θ_2 and is clearly consistent with θ_2 small, although the accuracy leaves something to be desired.

11.2 The amount of strange sea

The amount of the sea is determined from the *shape* of the neutrino and antineutrino x distributions. According to Eqs. (1) and (2), and given the fact stated in Section 9 that the x dependence of s(x) is experimentally consistent with the x dependence of $\bar{u}(x) + \bar{d}(x)$, it should be possible according to Eq. (1) to fit the neutrino x distribution with a mixture of xs(x) as given by the antineutrino x distribution and $x[u(x) + d(x)] \simeq \frac{1}{2}[F_2(x) + xF_3(x) - 2xs(x)]$.

Good fits are indeed obtained (see Fig. 10b), and give the results of Table 4, where r_{sea} and r_q are the slow rescaling factors for sea and quark distributions, respectively.

The experimental result for $2S/(U+D)$ is converted into the more interesting result for the ratio of strange to non-strange seas $2S/(\bar{U}+\bar{D})$ on the basis of the results obtained in the charged-current neutrino experiments [10], $\bar{U} + \bar{D} + 2\bar{S} = 0.070 \pm 0.005$ and $\int F_2(x)\,dx = 0.438 \pm 0.022$, as well as the result of this experiment, $2S/(U+D) = 0.052 \pm 0.004$ without the correction for slow rescaling.

With these values $(\bar{U}+\bar{D})/(U+D) = 0.13 \pm 0.02$ †). The final result, averaged over neutrino energy, is

$$\frac{|U_{cs}^2|}{U_{cd}^2} \; \frac{2S}{(\bar{U}+\bar{D})} = 9.3 \pm 1.6 \; . \qquad (6)$$

If, consistent with the preceding result on θ_2, we assume θ_2 small and also assume θ_3 small in line with the results of the comparisons of β, muon, and K decays [13], so that $U_{cd}^2/|U_{cs}^2| = \tan^2\theta_c = 0.056 \pm 0.005$, then the result for the amount of strange sea relative to the up-down sea becomes:

$$2S/(\bar{U}+\bar{D}) = 0.52 \pm 0.09 \; . \qquad (7)$$

A 10% variation in the value of m_c used in the slow rescaling correction changes this result by 5%, in the same direction. Subject to the above assumptions concerning the mixing angles, and after slow rescaling correction, the strange quark carries less of the nucleon momentum than the up or down antiquarks by a factor of about two. If the sea were flavour symmetric, we should have expected equal strange

†) This is the result of an iterative procedure based on $[|U_{cs}^2|/U_{cd}^2]\,[2S/(U+D)] = 0.92 \pm 0.06$ and $U_{cd}^2/|U_{cs}^2| = \tan^2\theta_c = 0.056 \pm 0.005$.

and up and down seas. The observation of non-symmetry, if not due to an inadequacy of the analysis, must then be attributed to some breakdown in the symmetry, perhaps to a difference in the strange quark and the up and down quark masses. From this result we can also obtain a limit on the coupling strength $|U_{cs}|$ of charmed and strange quarks. The maximum value for the strange-sea momentum fraction is reached for the symmetric case, $2S = \bar{U} + \bar{D}$. From Eq. (6) it follows that $|U_{cs}^2| \geq$ $\geq (9.3 \pm 1.6)\ U_{cd}^2$, and therefore $|U_{cs}| > 0.59$ at the 90% confidence level.

12. CONCLUSIONS

The main results of this work are the following:

i) Neutrino- and antineutrino-induced dimuon events show all the properties expected for a charged-current reaction and charm production and decay.

ii) The chirality of the weak charm-changing charged current is consistent with being V - A; a 95% confidence level upper limit of 0.07 is obtained for the square of the relative coupling strength of left-handed currents.

iii) The charm-fragmentation function D(z) is peaked at large values of z with an average of $\langle D(z) \rangle = 0.68 \pm 0.08$.

iv) Two elements of the Kobayashi-Maskawa matrix have been determined, $U_{cd} =$ $= 0.24 \pm 0.03$ and $|U_{cs}| > 0.59$ at the 90% confidence level.

v) For the Kobayashi-Maskawa angle θ_2 a value of $\cos \theta_2 = 1.05 \pm 0.14$ is obtained.

vi) The sea of strange quarks carries 52 ± 9% of the momentum of $\bar{u}$ or $\bar{d}$ quarks if the angles θ_2 and θ_3 are small.

REFERENCES

1. Benvenuti, A. et al.: Phys. Rev. Lett. 34, 419 (1975).
   Benvenuti, A. et al.: Phys. Rev. Lett. 35, 1199 (1975).
   Benvenuti, A. et al.: Phys. Rev. Lett. 41, 1204 (1978).
2. Barish, B.C. et al.: Phys. Rev. Lett. 36, 939 (1976).
   Barish, B.C. et al.: Phys. Rev. Lett. 39, 981 (1977).
3. Holder, M. et al.: Phys. Lett. 69B, 377 (1977).
4. Blietschau, J. et al.: Phys. Lett. 58B, 361 (1975).
   Blietschau, J. et al.: Phys. Lett. 60B, 207 (1976).
   Bosetti, B.C. et al.: Phys. Lett. 73B, 380 (1978).
5. Von Krogh, J. et al.: Phys. Rev. Lett. 36, 710 (1976).
   Bosetti, B.C. et al.: Phys. Rev. Lett. 38, 1248 (1977).
6. Baltay, C. et al.: Phys. Rev. Lett. 39, 62 (1977).
7. Jonker, M. et al.: Phys. Lett. 107B, 241 (1981).
8. Holder, M. et al.: Nucl. Instrum. Methods 148, 235 (1978).
9. Kobayashi, M., Maskawa, K.: Progr. Theor. Phys. 49, 652 (1973).
10. De Groot, J.G.H. et al.: Z. Phys. C1, 143 (1979).
    Abramowicz, H. et al.: Neutrino and antineutrino charged-current inclusive scattering in iron in the energy range $20 < E_\nu < 300$ GeV, to be published in Z. Phys. C.
11. De Groot, J.G.H. et al.: Phys. Lett. 86B, 103 (1979).
12. Glashow, S.L., Iliopoulos, J., Maiani, L.: Phys. Rev. D2, 1285 (1970).
13. Shrock, R.E., Wang, L.L.: Phys. Rev. Lett. 41, 1692 (1978) and 42, 1589 (1979).
14. Brock, R.: Phys. Rev. Lett. 44, 1027 (1980).
15. Bacino, W. et al.: Phys. Rev. Lett. 43, 1073 (1979).
16. Bjorken, J.D.: Phys. Rev. D 17, 171 (1978); Suzuki, M.: Phys. Lett. 71B, 139 (1977); Georgi, H., Politzer, H.D.: Nucl. Phys. B136, 445 (1978).
17. Ballagh, H.C. et al.: Phys. Rev. D 24, 7 (1981).
18. Baltay, C.: Recent results from neutrino experiment in heavy neon bubble chambers in Proc. 1979 JINR-CERN School of Physics, September 1979, p. 72. Budapest: Hungarian Academy of Sciences, 1980.

19. Stanton, N. et al.: E531 Collaboration in Neutrino 81, Proc. 11th Int. Conf. on Neutrino Physics and Astrophysics, Maui, Hawaii, 1981, p. 491. Honolulu: Dept. of Phys. and Astrophys., Univ. of Hawaii, 1981.

Fisk, E.: Rapporteur's talk, in Proc. Int. Symposium on Lepton and Photon Interactions at High Energy, Bonn, 1981, p. 703. Bonn: Universität Bonn, 1981.

20. Feller, J.M. et al.: Phys. Rev. Lett. 40, 274 (1978).

21. Schindler, R.H.: Ph.D. Thesis, SLAC report 219 (1979).

22. Roos, M., as quoted by Kleinknecht, K.: in Proc. 17th Int. Conf. on High Energy Physics, London, England, 1974, p. III-23. Chilton, Didcot, Berks.: Rutherford High Energy Laboratory, 1975, and by Nagel, M. et al.: Nucl. Phys. B109, 1 (1976). See also Roos, M.: Nucl. Phys. B77, 420 (1974).

Table 1

Antineutrino- and neutrino-induced dimuon events, $N_{\bar{\nu}}$ and N_{ν}, as obtained from the antineutrino WBB after separation and correction for migration

Visible energy (GeV)	$N_{\bar{\nu}}$	N_{ν}
30–40	261	69
40–60	534	194
60–80	523	212
80–100	353	185
100–120	200	163
120–140	113	130
140–160	70	89
160–200	55	85

Table 2

Number of observed neutrino-induced (N_{-+}) and antineutrino-induced (N_{+-}) dimuon events, together with normalized single-muon event rates, N_- and N_+

E_{vis}	ν		$\bar{\nu}$	
(GeV)	N_{-+}	$N_- \times 10^{-6}$	N_{+-}	$N_+ \times 10^{-6}$
30–40	749	1.9	261	0.54
40–60	1850	1.49	534	0.51
60–80	2037	1.00	523	0.25
80–100	1697	0.71	353	0.17
100–120	1306	0.47	200	0.08
120–140	876	0.27	113	0.04
140–160	694	0.17	70	0.02
160–180	338	0.09	38	
180–200	195	0.04	17	0.01
200–240	189	0.04	9	
> 240	91	0.01	5	
30–500	9922	6.19	2123	1.62

Table 3

Dimuon to single-muon cross-section ratios
(corrected for slow rescaling)
and the quantity $U_{cd}^2 B$ (in units of 10^{-2})

E_ν (GeV)	$\sigma^{\nu}_{\mu^-\mu^+}/\sigma^{\nu}_{\mu^-}$	$\sigma^{\bar{\nu}}_{\mu^+\mu^-}/\sigma^{\bar{\nu}}_{\mu^+}$	$U_{cd}^2 B$
30-40	0.36 ± 0.05	0.73 ± 0.08	0.01 ± 0.12
40-60	0.67 ± 0.04	1.02 ± 0.07	0.23 ± 0.10
60-80	0.78 ± 0.04	1.13 ± 0.06	0.30 ± 0.10
80-100	0.82 ± 0.06	1.12 ± 0.09	0.36 ± 0.13
100-120	0.81 ± 0.04	1.06 ± 0.10	0.39 ± 0.11
120-140	0.88 ± 0.05	1.05 ± 0.12	0.48 ± 0.14
140-160	0.83 ± 0.07	1.02 ± 0.13	0.43 ± 0.17
80-160	0.83 ± 0.025	1.07 ± 0.05	0.41 ± 0.07

Table 4

The fraction of strange sea

E_ν (GeV)	r_{sea}	r_q	$\frac{\lvert U_{cs}^2\rvert}{U_{cd}^2}\frac{2S}{U+D}$	$\frac{\lvert U_{cs}^2\rvert}{U_{cd}^2}\frac{2S}{\bar{U}+\bar{D}}$	$\frac{2S}{\bar{U}+\bar{D}}$ for $\frac{U_{cd}^2}{\lvert U_{cs}^2\rvert} = 0.056$
35-60	2.11	1.33	1.10 ± 0.16	8.6 ± 1.8	0.48 ± 0.10
60-110	1.53	1.19	1.34 ± 0.10	10.5 ± 1.8	0.59 ± 0.10
110-160	1.36	1.13	1.23 ± 0.17	9.6 ± 2.0	0.54 ± 0.11
> 160	1.24	1.10	1.36 ± 0.20	10.6 ± 2.2	0.59 ± 0.12
> 35	1.53	1.19	1.19 ± 0.09	9.3 ± 1.6	0.52 ± 0.09

Figure captions

Fig. 1 : Neutrino spectra in (a) neutrino and (b) antineutrino WBBs.

Fig. 2 : Scatter plot of p_T^+ versus p_T^- for dimuons from (a) neutrino and (b) antineutrino beams. p_T is the transverse momentum of the muon relative to the hadron shower direction.

Fig. 3 : Calculated background contribution from π and K decays for 350 GeV neutrino and antineutrino WBBs.

Fig. 4 : Kinematical distributions (a) and (b) neutrino and (c) and (d) antineutrino dimuon events. The variables are defined in the text. The dashed area represents the π and K background which has been subtracted from the raw data. The curves are results of the Monte Carlo simulation.

Fig. 5 : Energy spectrum of (a) dimuon events and (b) single-muon events for different radial bins of the detector; 200 GeV NBB data (histogram). The points are the result of a Monte Carlo simulation.

Fig. 6 : E_ν/E_{vis} plotted as a function of E_{vis}. The points are the result of a fit to the dimuon energy spectra in radial bins (Fig. 5a). The curves are Monte Carlo results for 200 GeV NBB and 400 GeV WBB.

Fig. 7 : y distribution of observed neutrino events for (a) $30 \leq E_\nu \leq 50$ GeV and (b) $E_\nu > 150$ GeV; the solid and dashed curves represent the V - A current and V + A current, respectively, for charm production.

Fig. 8 : Distribution of neutrino dimuon events in the variable z_L compared with Monte Carlo results.

Fig. 9 : Charm fragmentation function D(z). Results of the fit in z_L and y_{had}.

Fig. 10 : x_{vis} distribution for dimuon events. The histograms represent the data. a) Antineutrino; the solid curve is the sea distribution obtained in our single-muon analysis (Ref. 10), the dashed-dotted curve demonstrates the effect of slow rescaling. b) Neutrino; the curves

show the decomposition into 48% strange-sea contribution taken from the data of Fig. 10a (dotted curve) and 52% quark contribution (dash-dotted curve). The dashed curve is the sum of both.

Fig. 11 : $R_2^{\nu} = \sigma^{\nu}(2\mu)/\sigma^{\nu}(1\mu)$ for neutrinos: a) raw data, b) acceptance corrected data. The solid error bars indicate statistical errors, the dotted error bars include systematic errors due to the uncertainty in the fragmentation function.

Fig. 12 : $R_2^{\bar{\nu}} = \sigma^{\nu}(2\mu)/\sigma^{\bar{\nu}}(1\mu)$ for antineutrinos: a) raw data, b) acceptance corrected data. Errors as for Fig. 11.

Fig. 13 : Acceptance for neutrino dimuon events for two fragmentation functions. Solid line $D_c(z) = \delta(z-0.68)$, dashed line $D_c(z) = \text{const.}$

Fig. 14 : Double ratio $\left[\sigma^{\bar{\nu}}(2\mu)/\sigma^{\bar{\nu}}(1\mu)\right]/\left[\sigma^{\nu}(2\mu)/\sigma^{\nu}(1\mu)\right]$ as a function of energy.

Fig. 15 : $R_2^{\nu} = \sigma^{\nu}(2\mu)/\sigma^{\nu}(1\mu)$ from this experiment and bubble-chamber results.

Fig. 16 : $R_2 = \sigma(2\mu)/\sigma(1\mu)$ corrected for slow rescaling: a) for neutrinos, b) for antineutrinos.

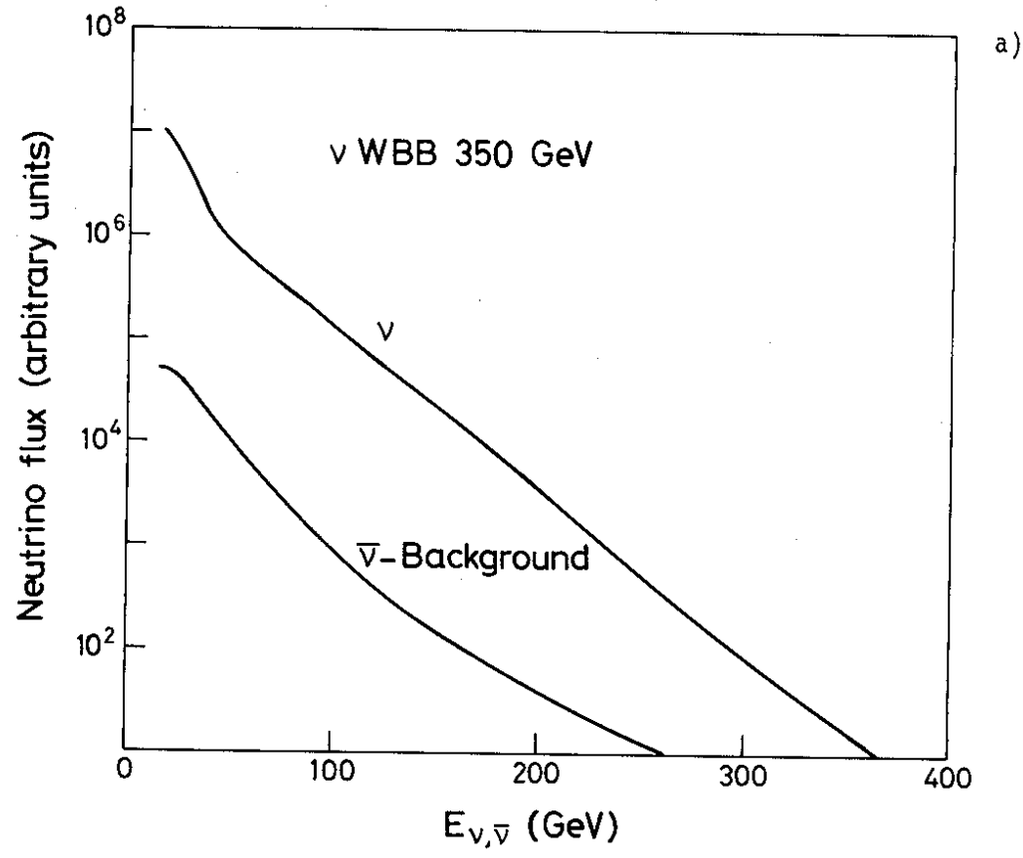
a)
ν WBB 350 GeV
ν
ν̄-Background
Neutrino flux (arbitrary units)
10^8
10^6
10^4
10^2
0
100
200
300
400
$E_{\nu,\bar{\nu}}$ (GeV)

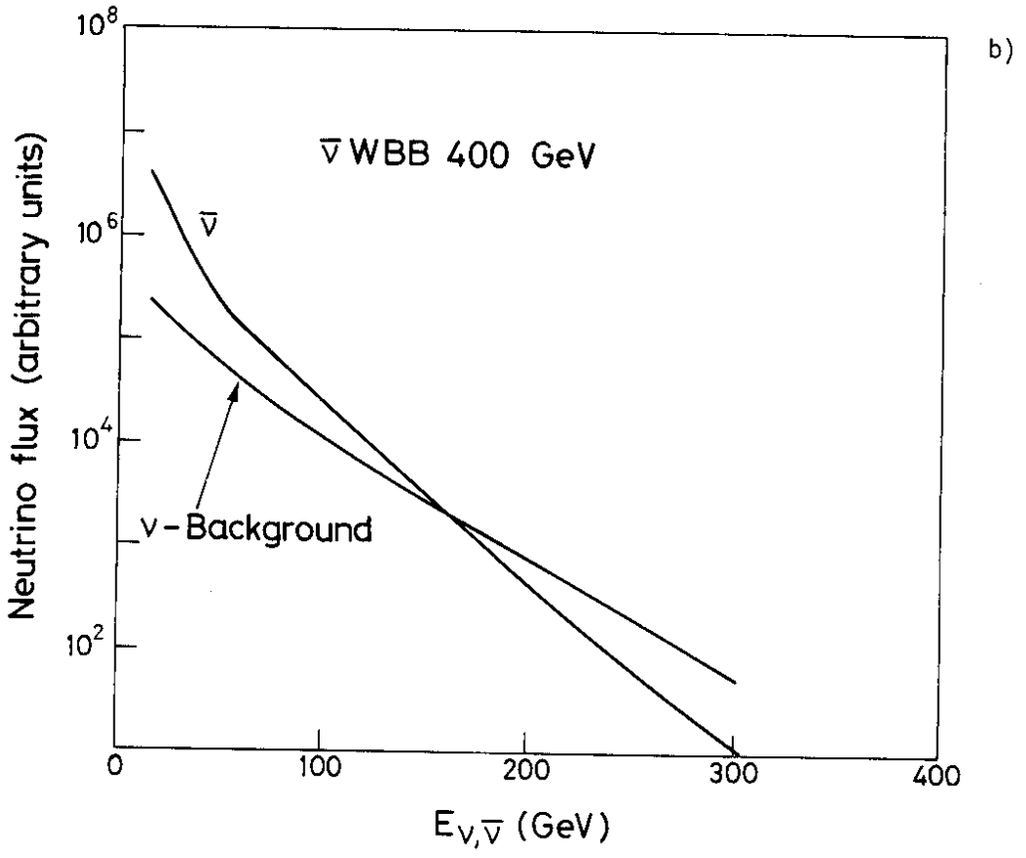
b)
ν̄ WBB 400 GeV
ν̄
ν-Background
Neutrino flux (arbitrary units)
10^8
10^6
10^4
10^2
0
100
200
300
400
$E_{\nu,\bar{\nu}}$ (GeV)

Fig. 1

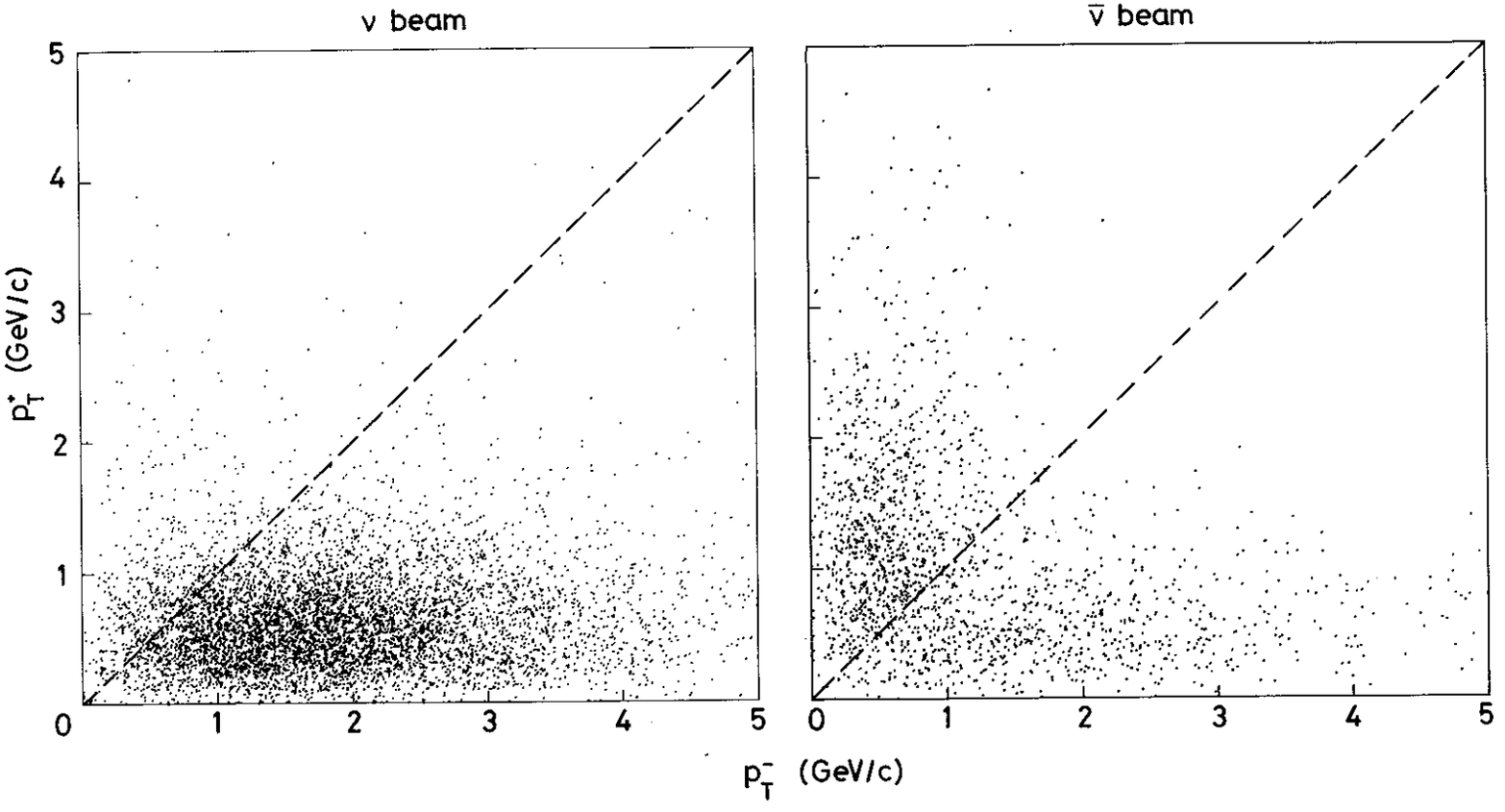

Fig. 2

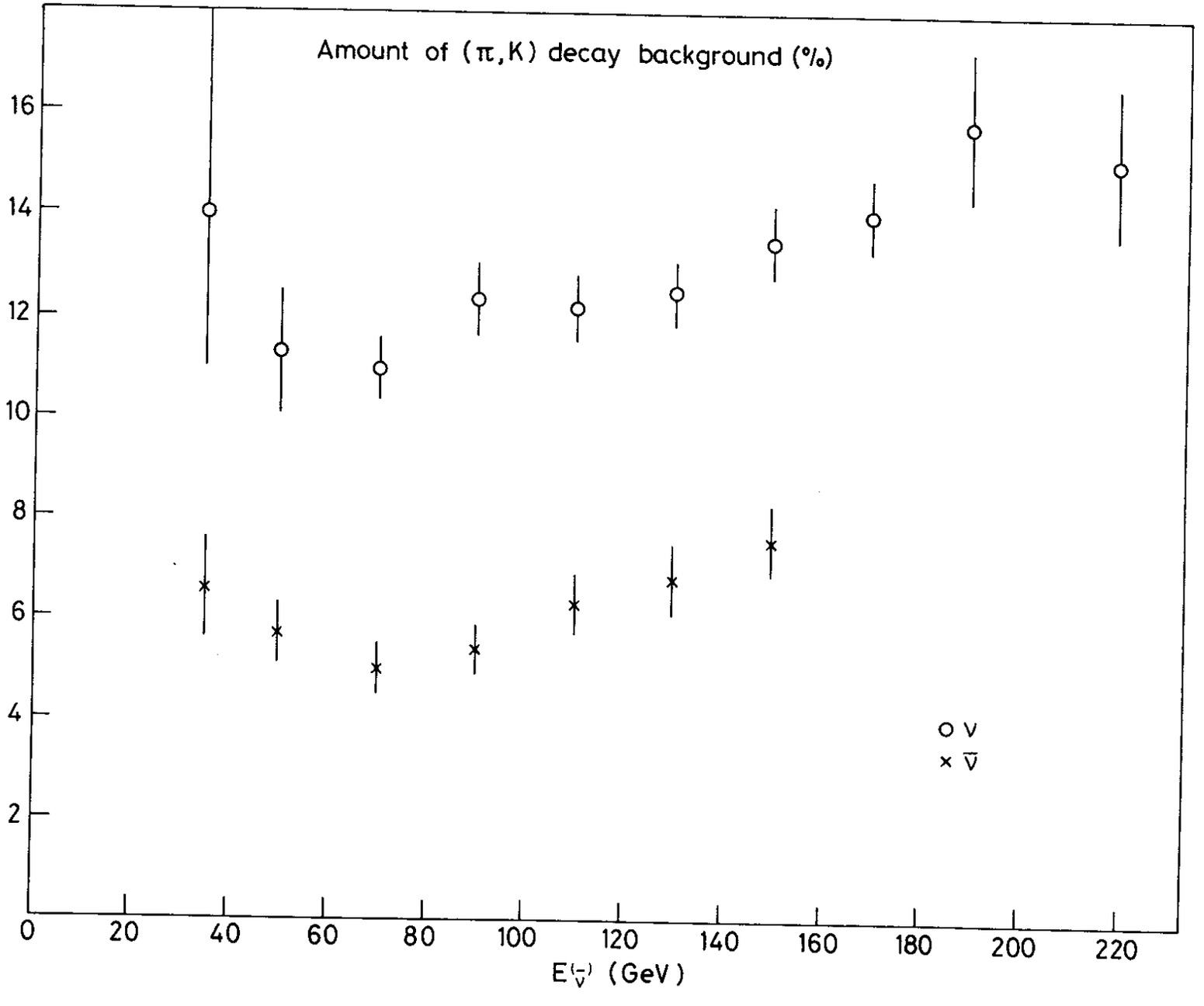
Amount of (π,K) decay background (%)
16
14
12
10
8
6
4
2
0
20
40
60
80
100
120
140
160
180
200
220
E(−)ν (GeV)
○ ν
× ν̄

Fig. 3

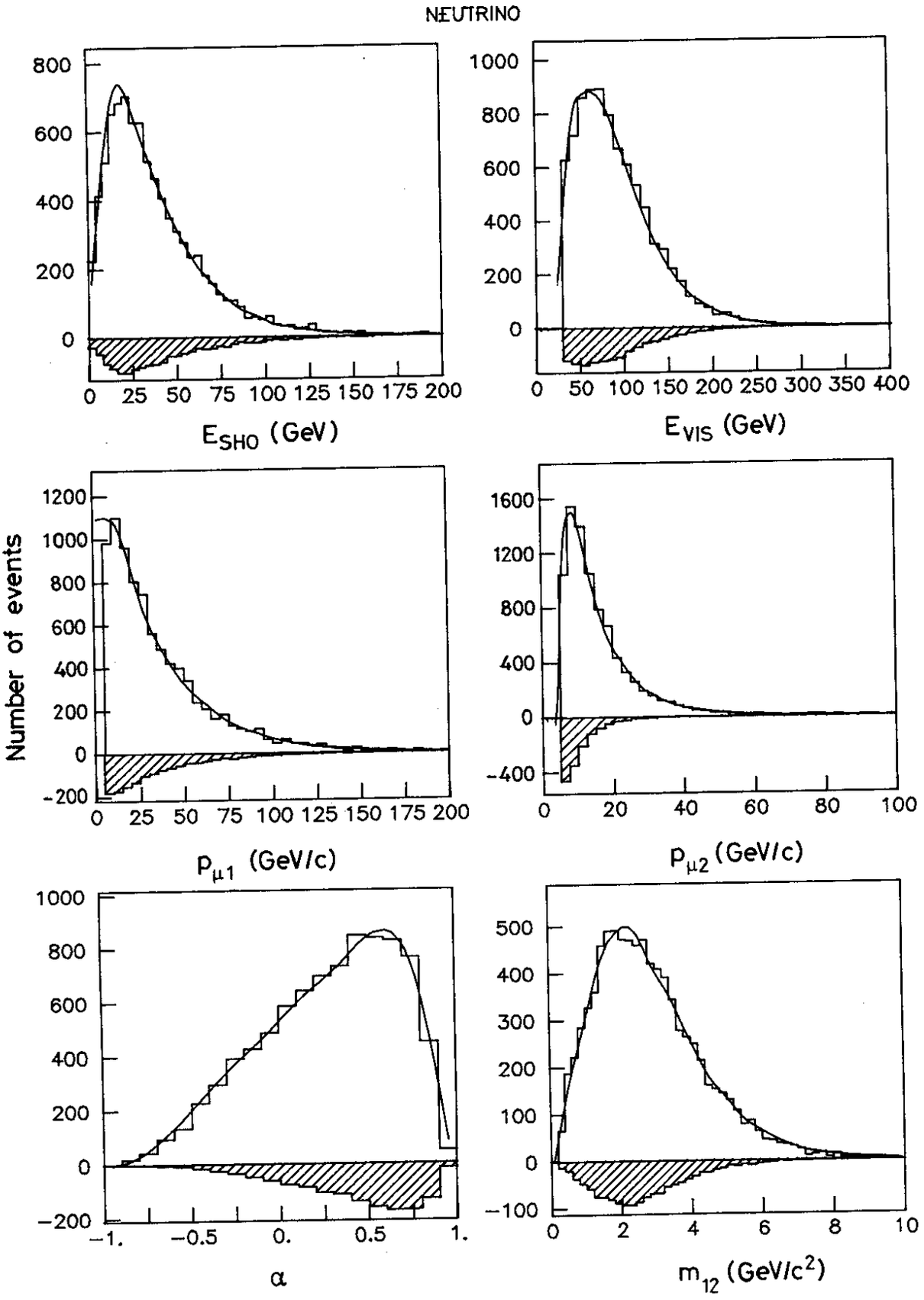
NEUTRINO
Number of events
E_{SHO} (GeV)
E_{VIS} (GeV)
$p_{\mu 1}$ (GeV/c)
$p_{\mu 2}$ (GeV/c)
α
m_{12} (GeV/c^2)

Fig. 4a

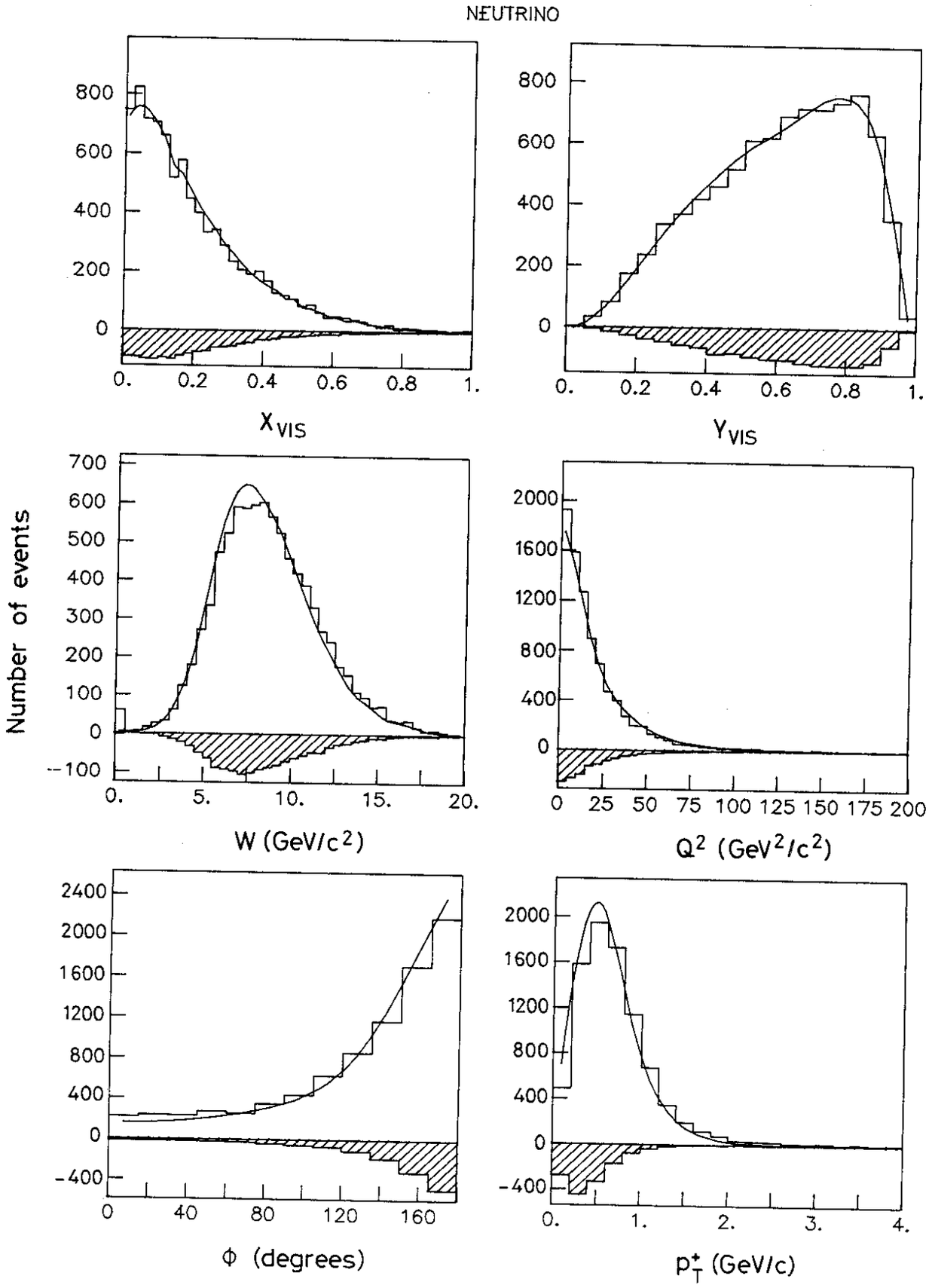
NEUTRINO
Number of events
X_{VIS}
Y_{VIS}
W (GeV/c^2)
Q^2 (GeV^2/c^2)
Φ (degrees)
p_T^+ (GeV/c)

Fig. 4b

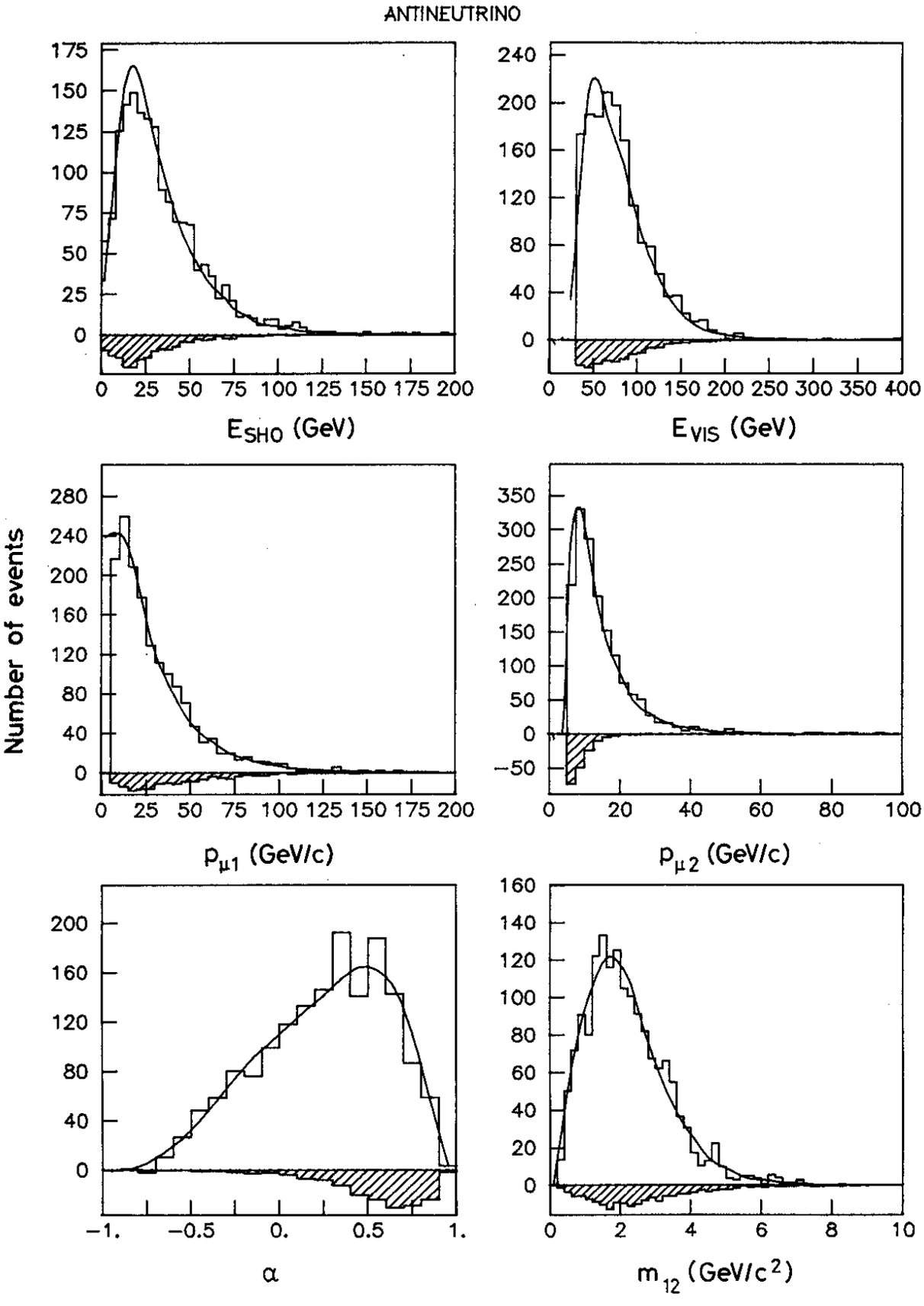
ANTINEUTRINO
Number of events
E_{SHO} (GeV)
E_{VIS} (GeV)
$p_{\mu 1}$ (GeV/c)
$p_{\mu 2}$ (GeV/c)
α
m_{12} (GeV/c^2)

Fig. 4c

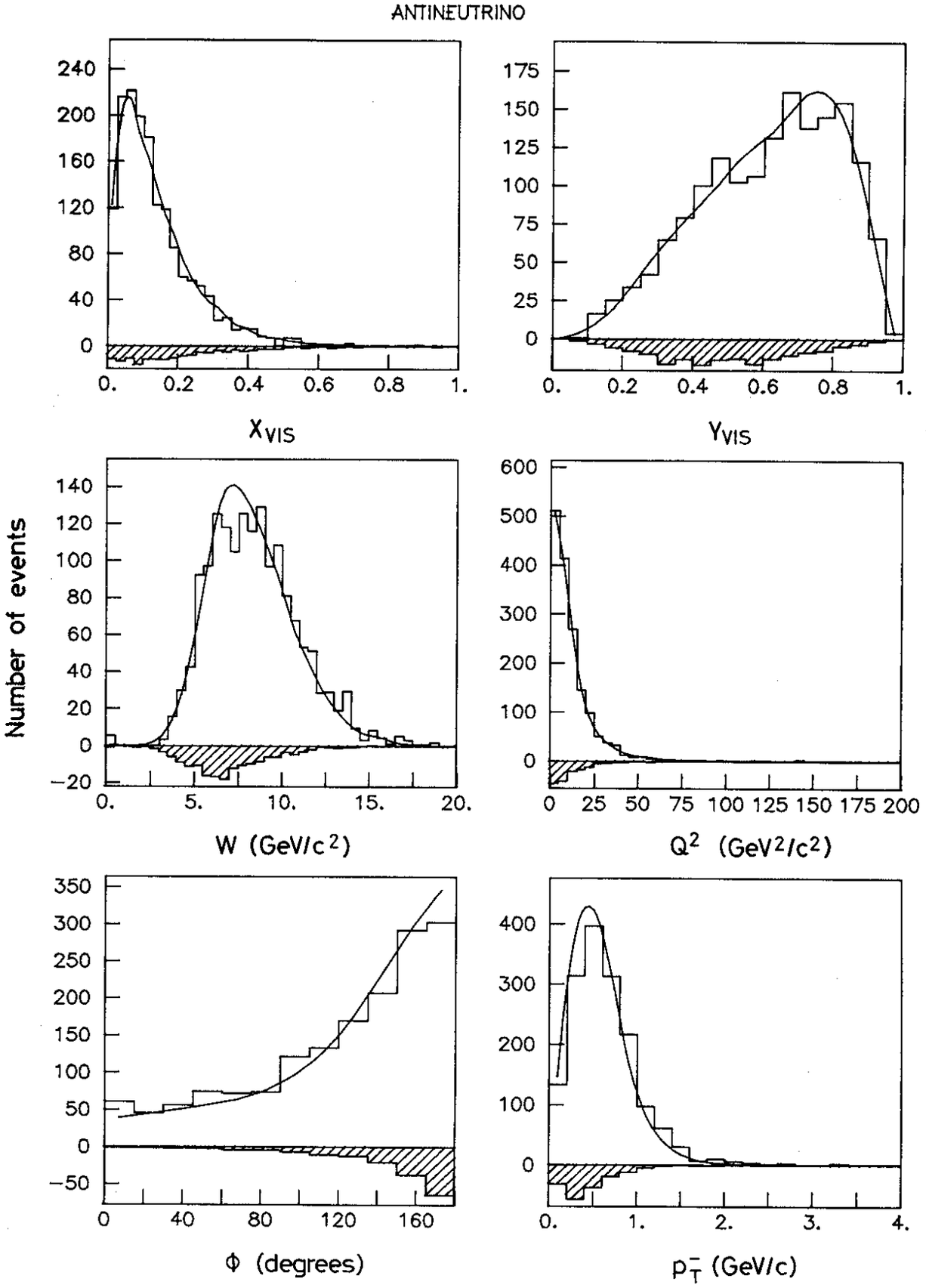
ANTINEUTRINO
Number of events
X_{VIS}
Y_{VIS}
W (GeV/c^2)
Q^2 (GeV^2/c^2)
Φ (degrees)
p_T^- (GeV/c)

Fig. 4d

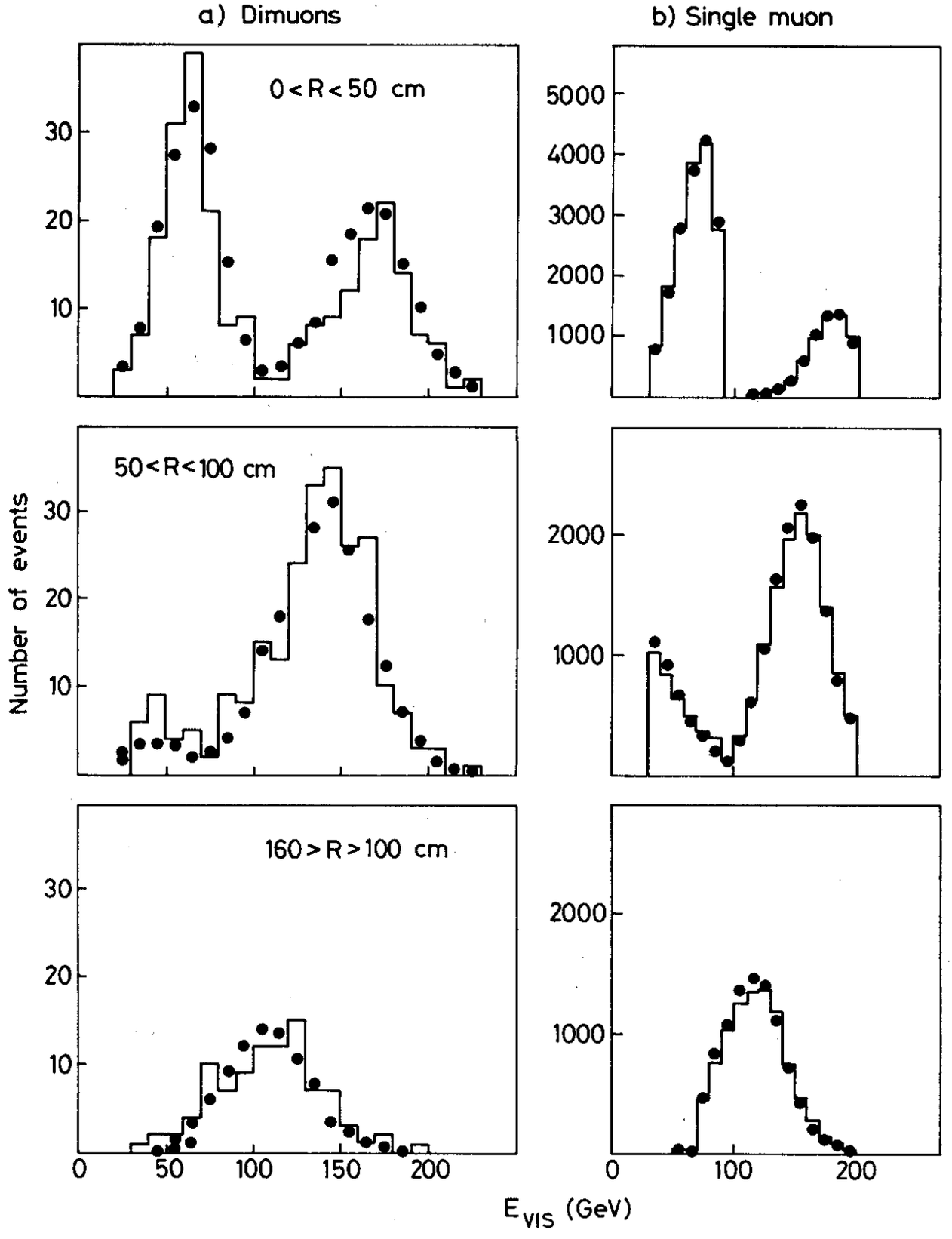
a) Dimuons
b) Single muon
0<R<50 cm
50<R<100 cm
160>R>100 cm
Number of events
E_{VIS} (GeV)

Fig. 5

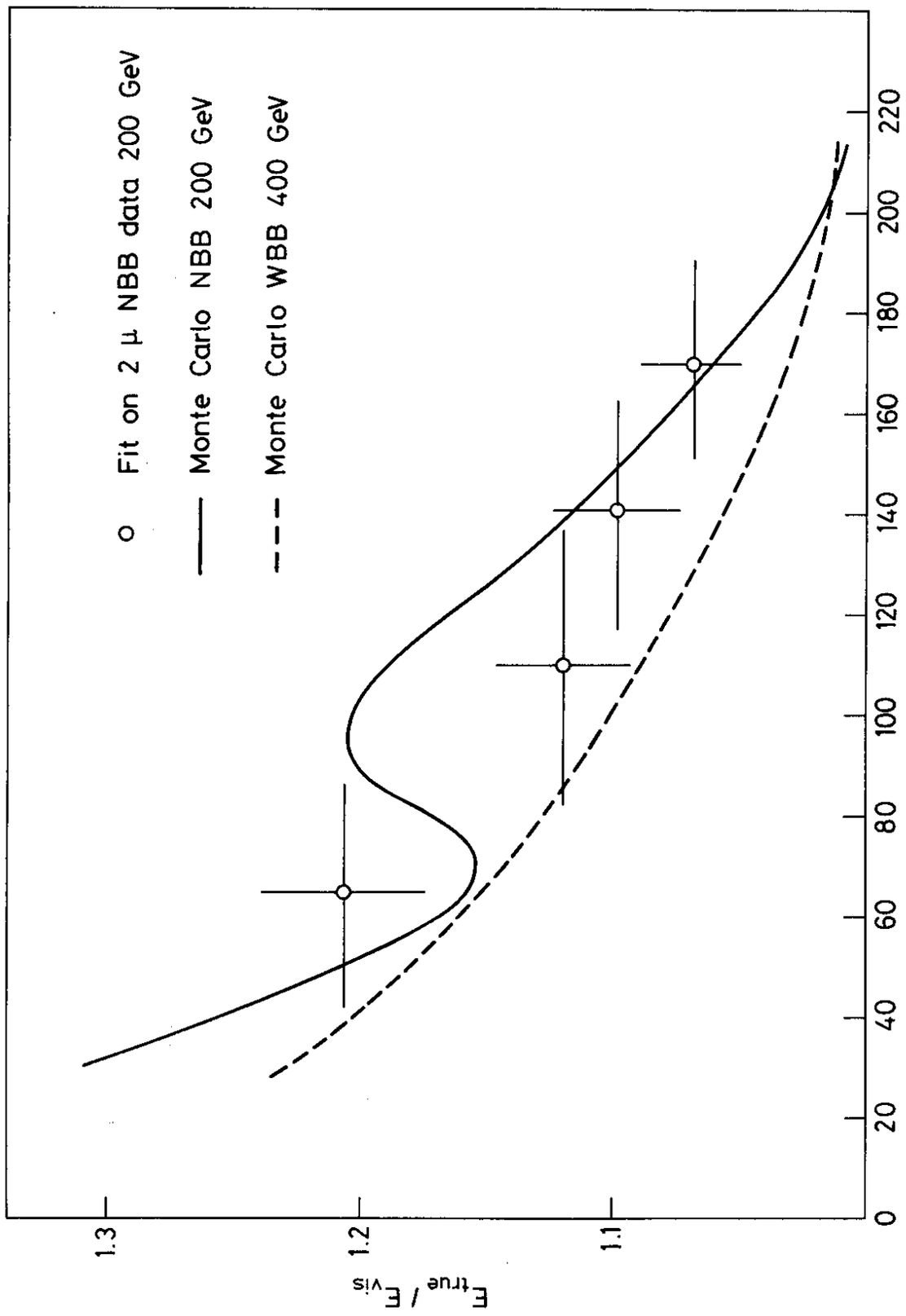
o Fit on 2 μ NBB data 200 GeV
Monte Carlo NBB 200 GeV
Monte Carlo WBB 400 GeV
E_{true} / E_{vis}
E_{vis}
1.3
1.2
1.1
0
20
40
60
80
100
120
140
160
180
200
220

Fig. 6

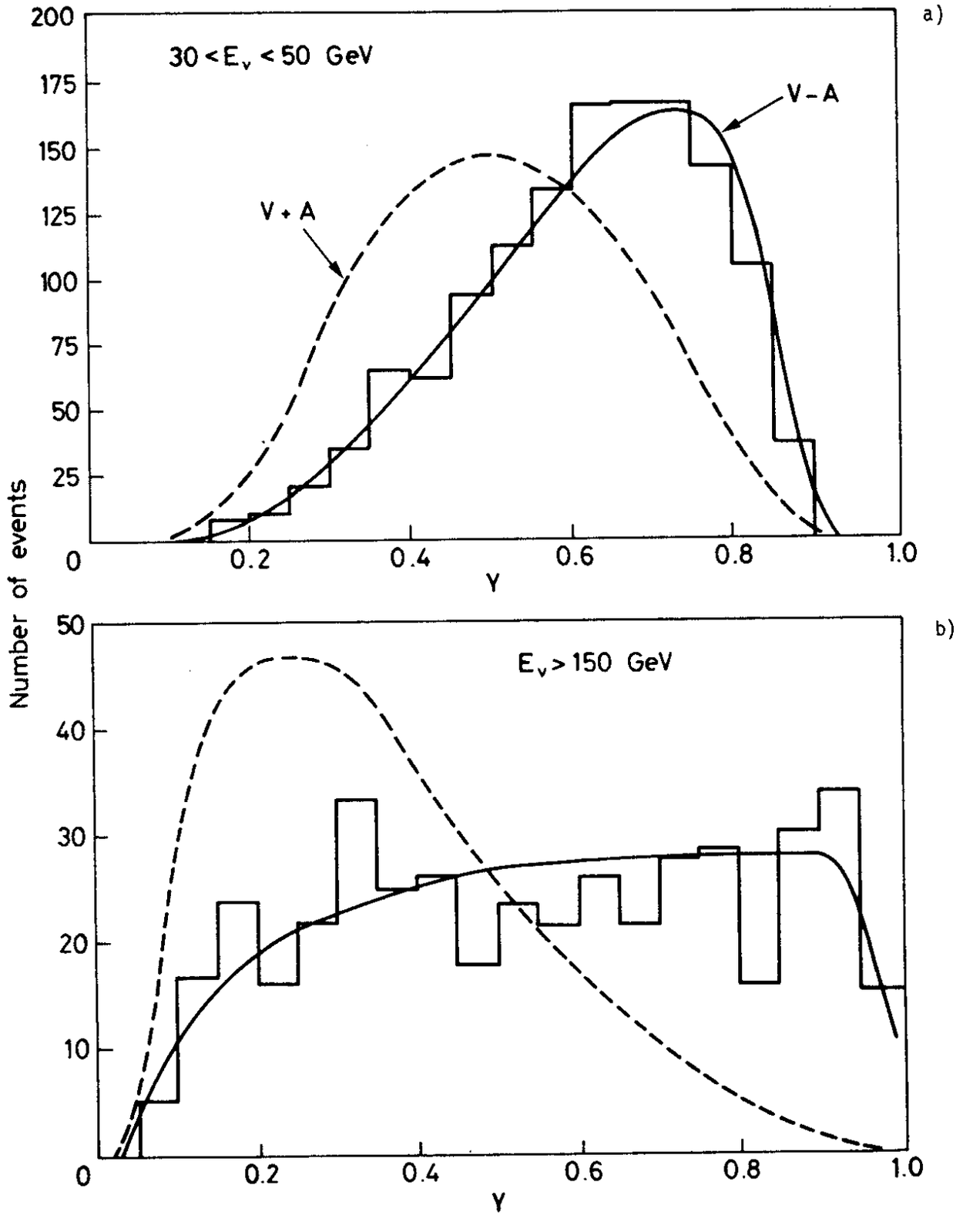
a)
$30 < E_\nu < 50$ GeV
V - A
V + A
200
175
150
125
100
75
50
25
0
0.2
0.4
0.6
0.8
1.0
Y
Number of events
b)
$E_\nu > 150$ GeV
50
40
30
20
10
0
0.2
0.4
0.6
0.8
1.0
Y

Fig. 7

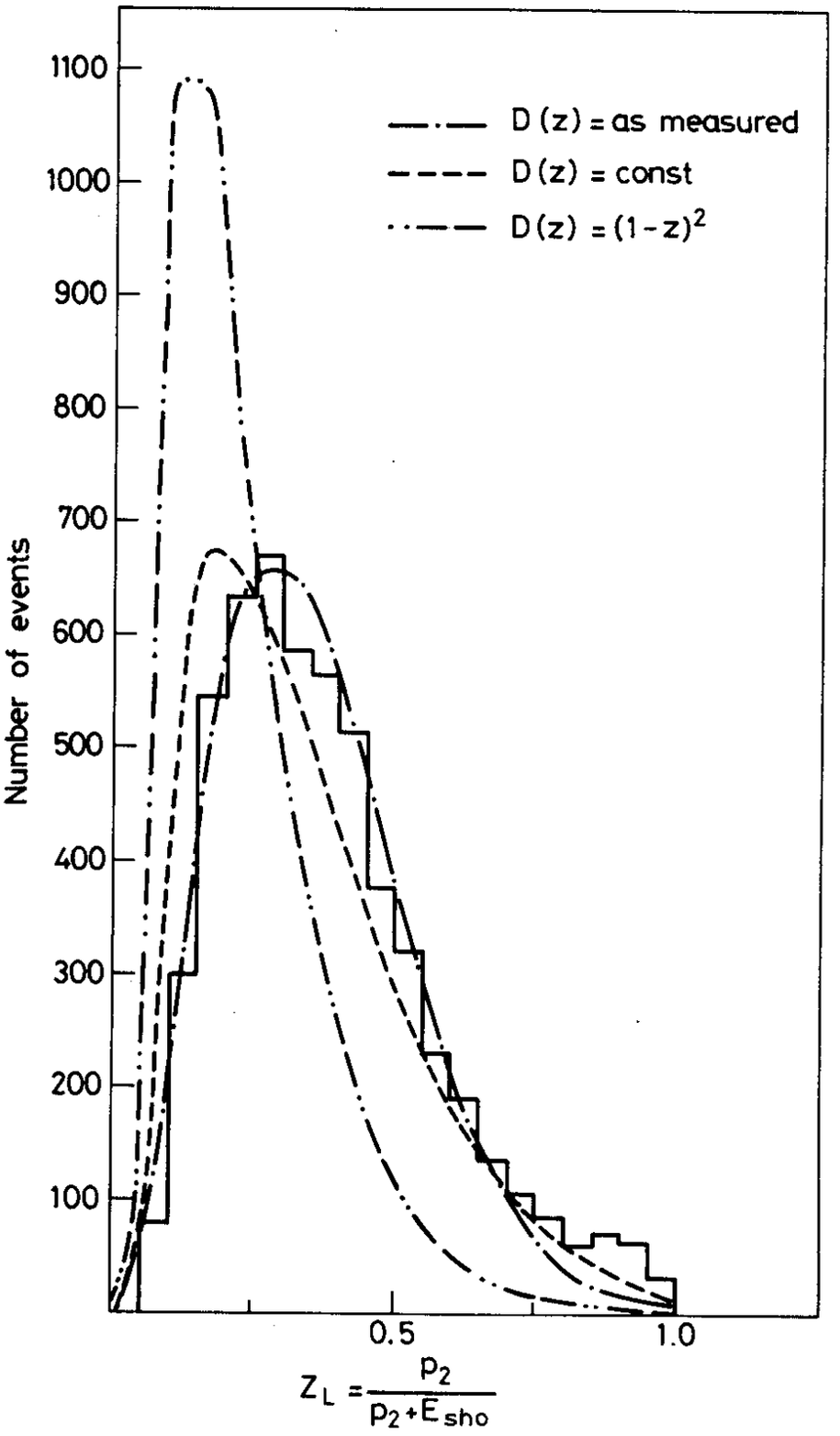
D(z) = as measured
D(z) = const
D(z) = (1-z)²
Number of events
1100
1000
900
800
700
600
500
400
300
200
100
0.5
1.0
$Z_L = \frac{p_2}{p_2 + E_{sho}}$

Fig. 8

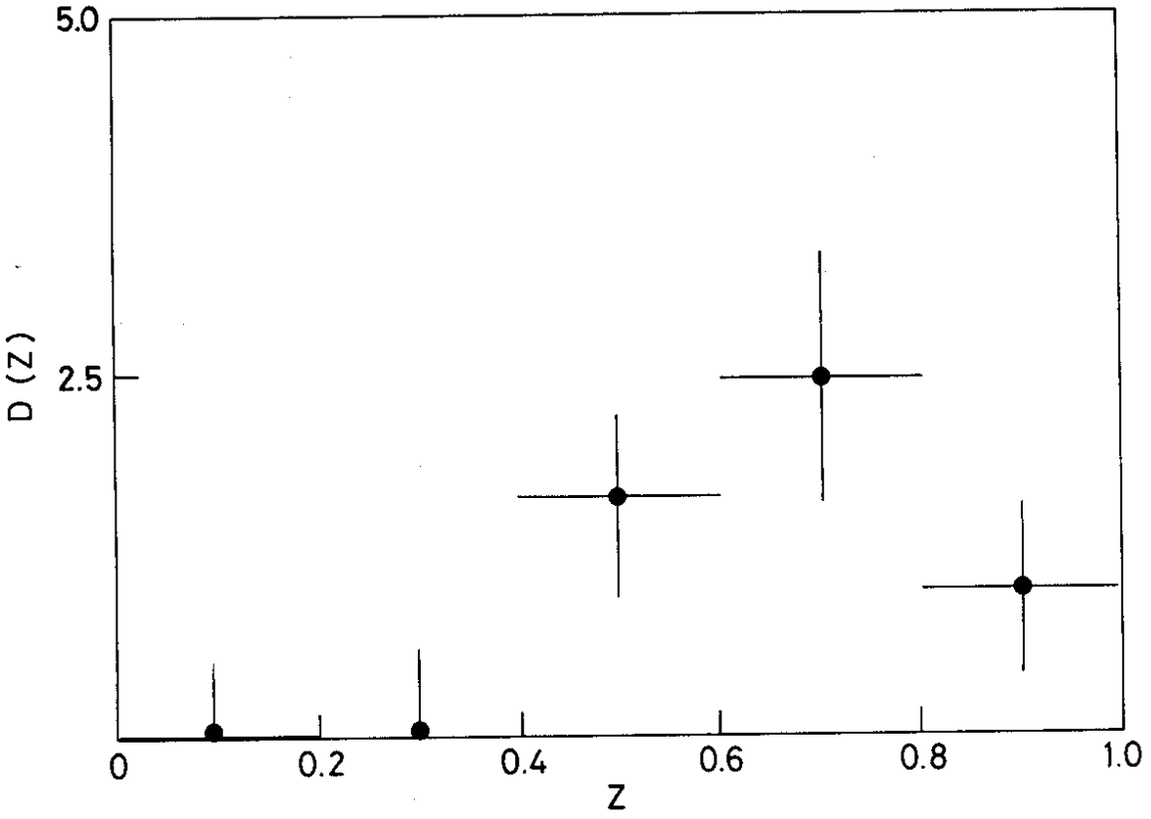

Fig. 9

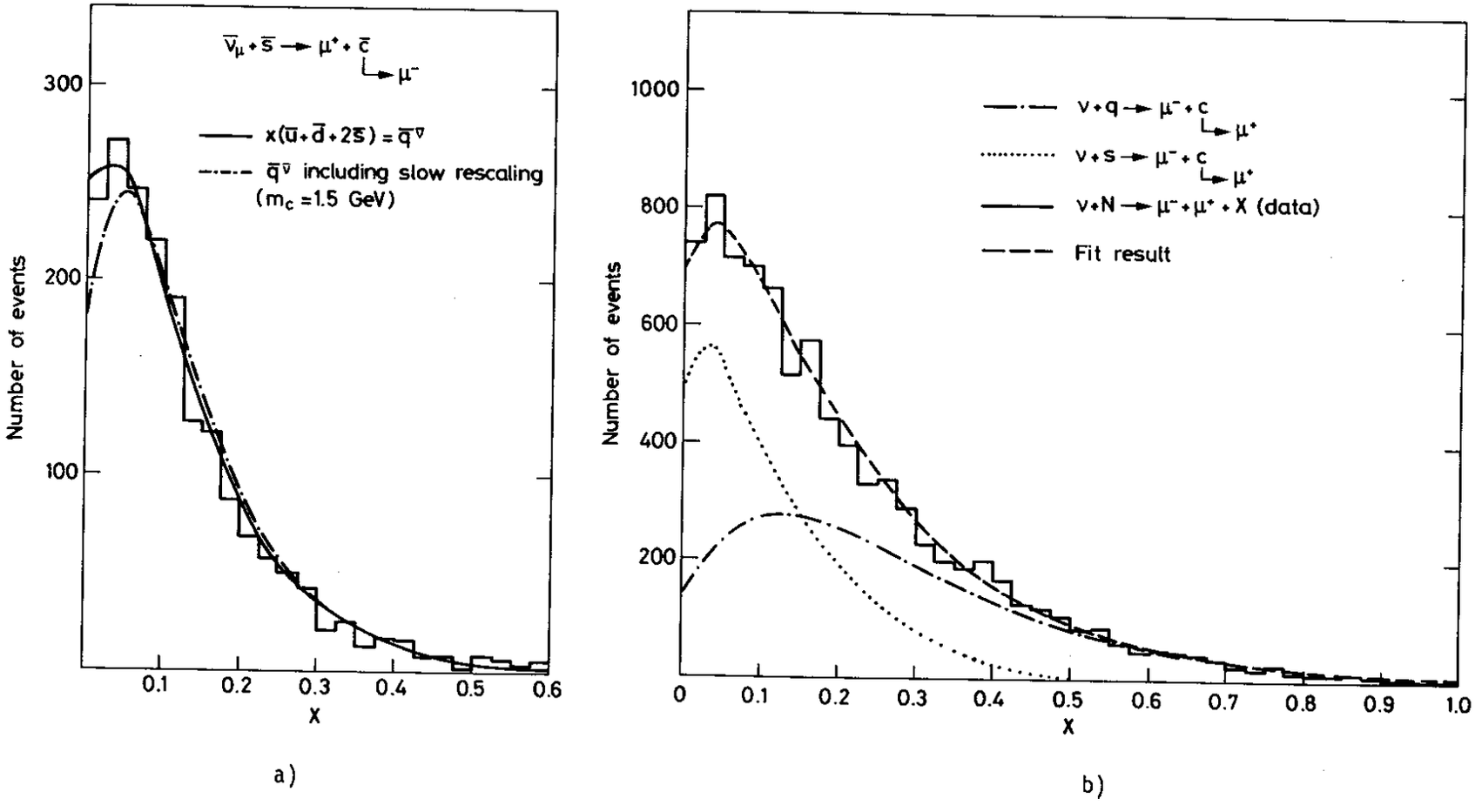
$\bar{\nu}_\mu + \bar{s} \rightarrow \mu^+ + \bar{c}$
$\hookrightarrow \mu^-$
$x(\bar{u}+\bar{d}+2\bar{s}) = \bar{q}^{\bar{\nu}}$
$\bar{q}^{\bar{\nu}}$ including slow rescaling
(m_c =1.5 GeV)
Number of events
X
a)
$\nu + q \rightarrow \mu^- + c$
$\hookrightarrow \mu^+$
$\nu + s \rightarrow \mu^- + c$
$\hookrightarrow \mu^+$
$\nu + N \rightarrow \mu^- + \mu^+ + X$ (data)
Fit result
Number of events
X
b)

Fig. 10

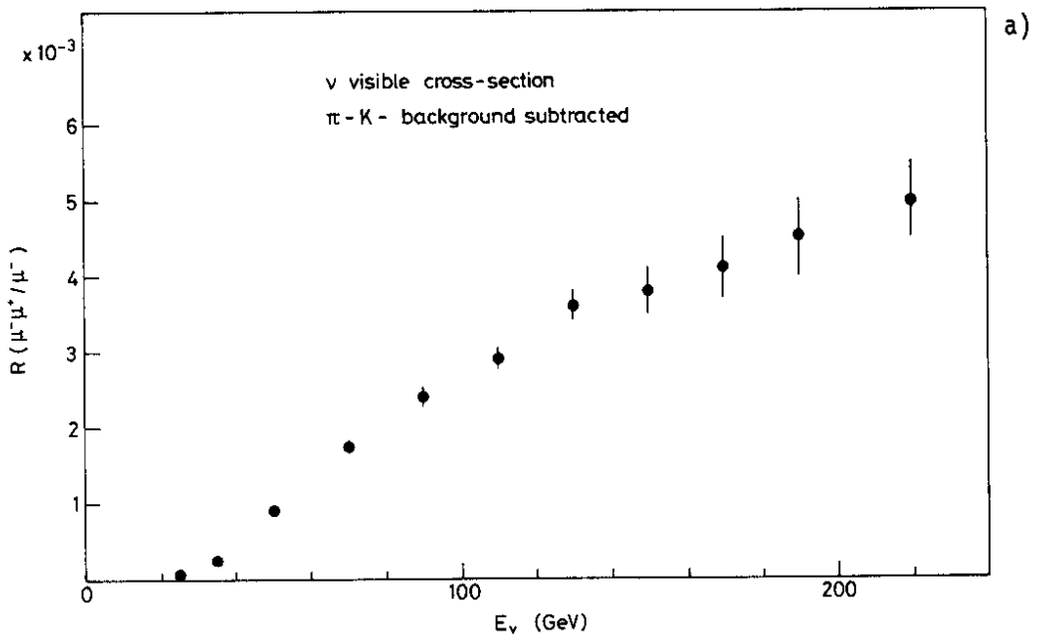
a)
x 10⁻³
ν visible cross-section
π - K - background subtracted
R (μ⁻μ⁺/μ⁻)
6
5
4
3
2
1
0
100
200
Eν (GeV)

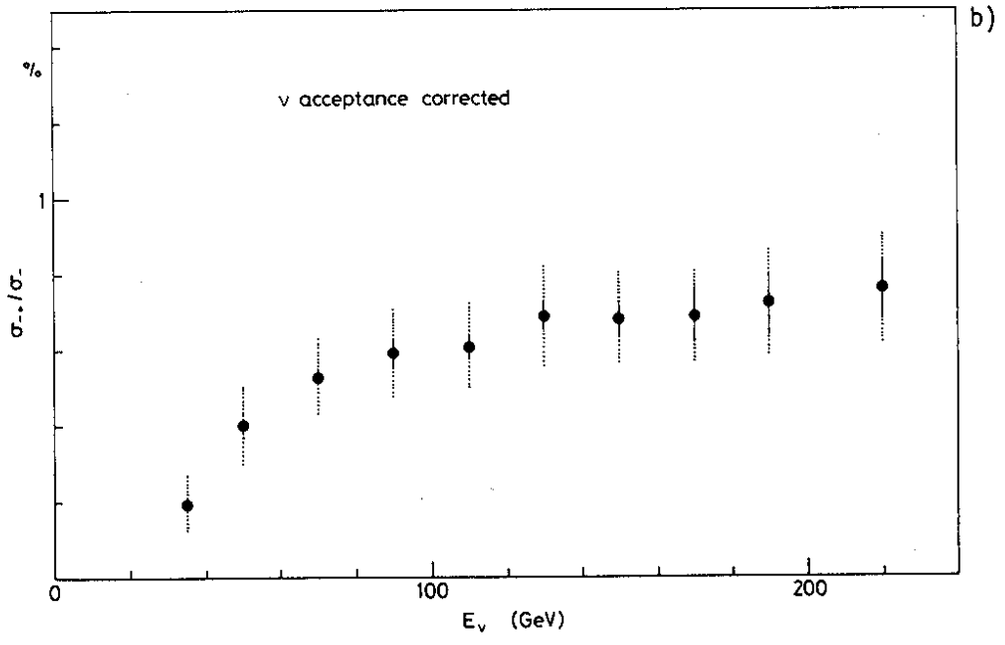
b)
%
ν acceptance corrected
σ-+/σ-
1
0
100
200
Eν (GeV)

Fig. 11

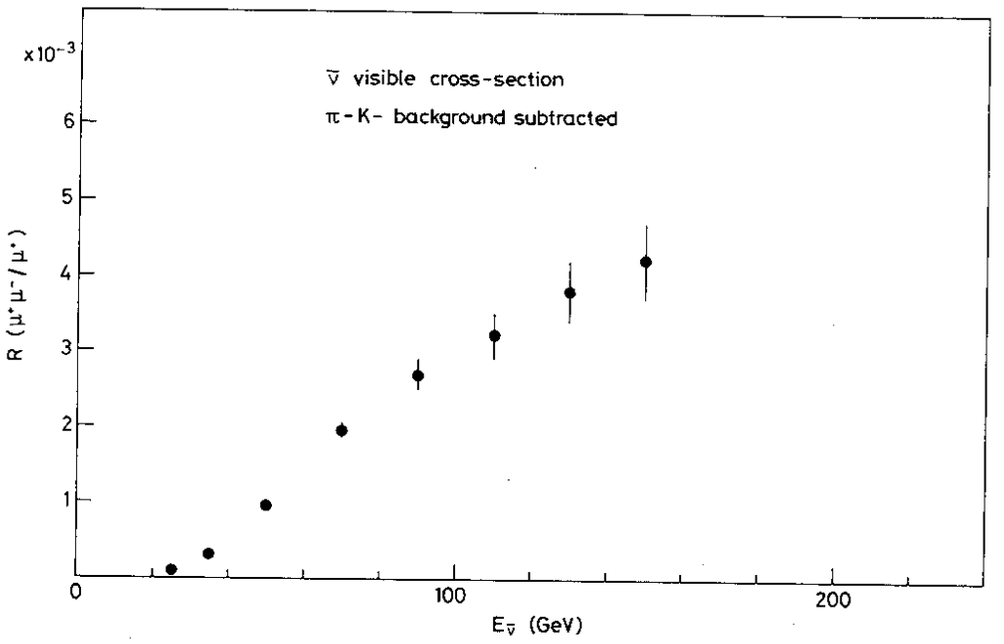
a)
x10⁻³
6
5
4
3
2
1
0
100
200
R (μ⁺μ⁻/μ⁺)
ν̄ visible cross-section
π-K- background subtracted
Eν̄ (GeV)

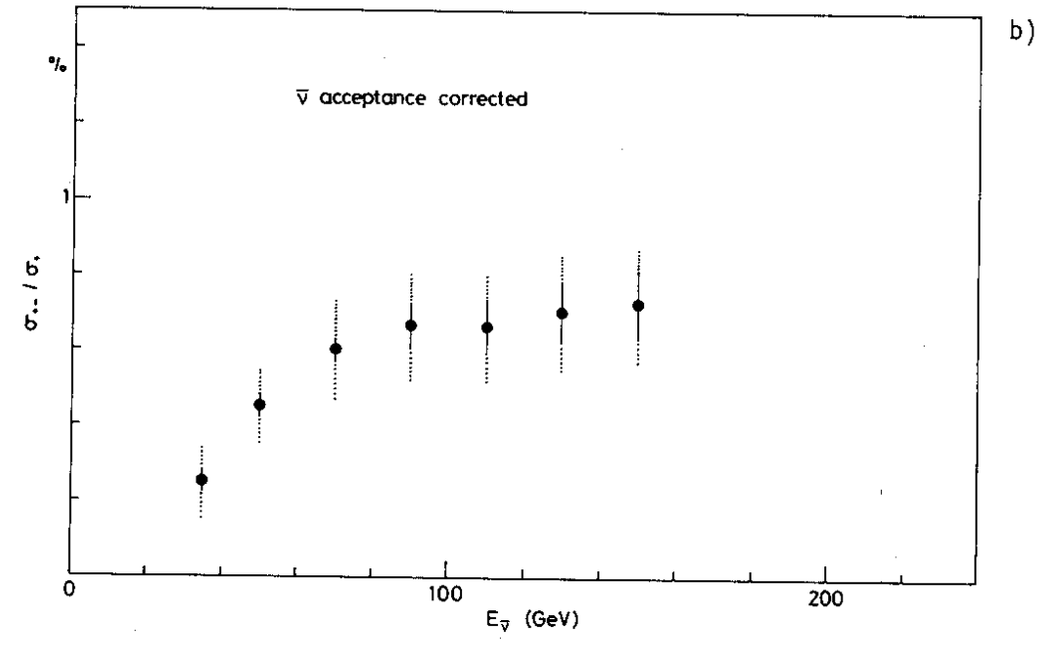
b)
%
1
0
100
200
σ₋₋ / σ₊
ν̄ acceptance corrected
Eν̄ (GeV)

Fig. 12

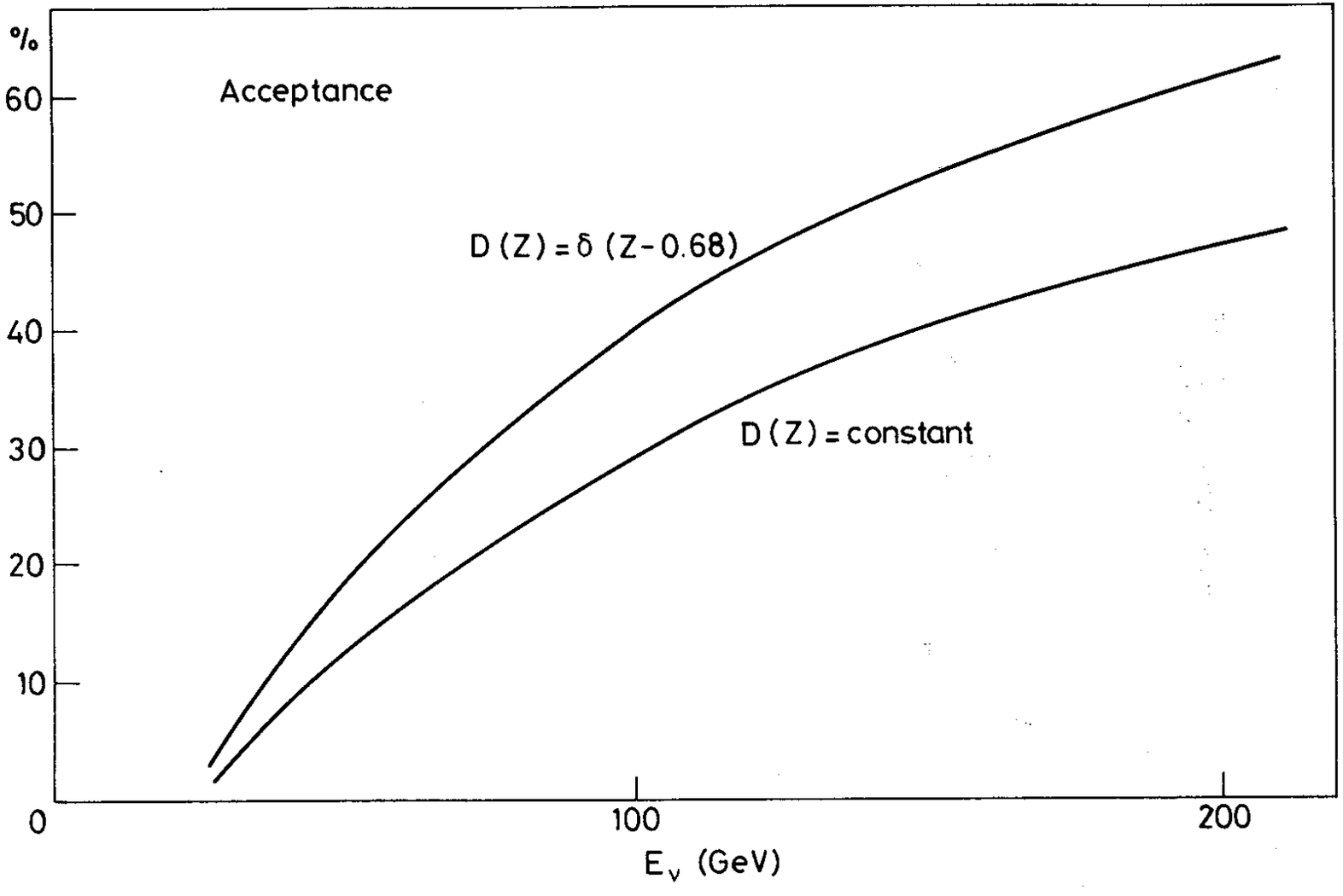
%
60
50
40
30
20
10
0
Acceptance
D (Z) = δ (Z - 0.68)
D (Z) = constant
100
200
E_ν (GeV)

Fig. 13

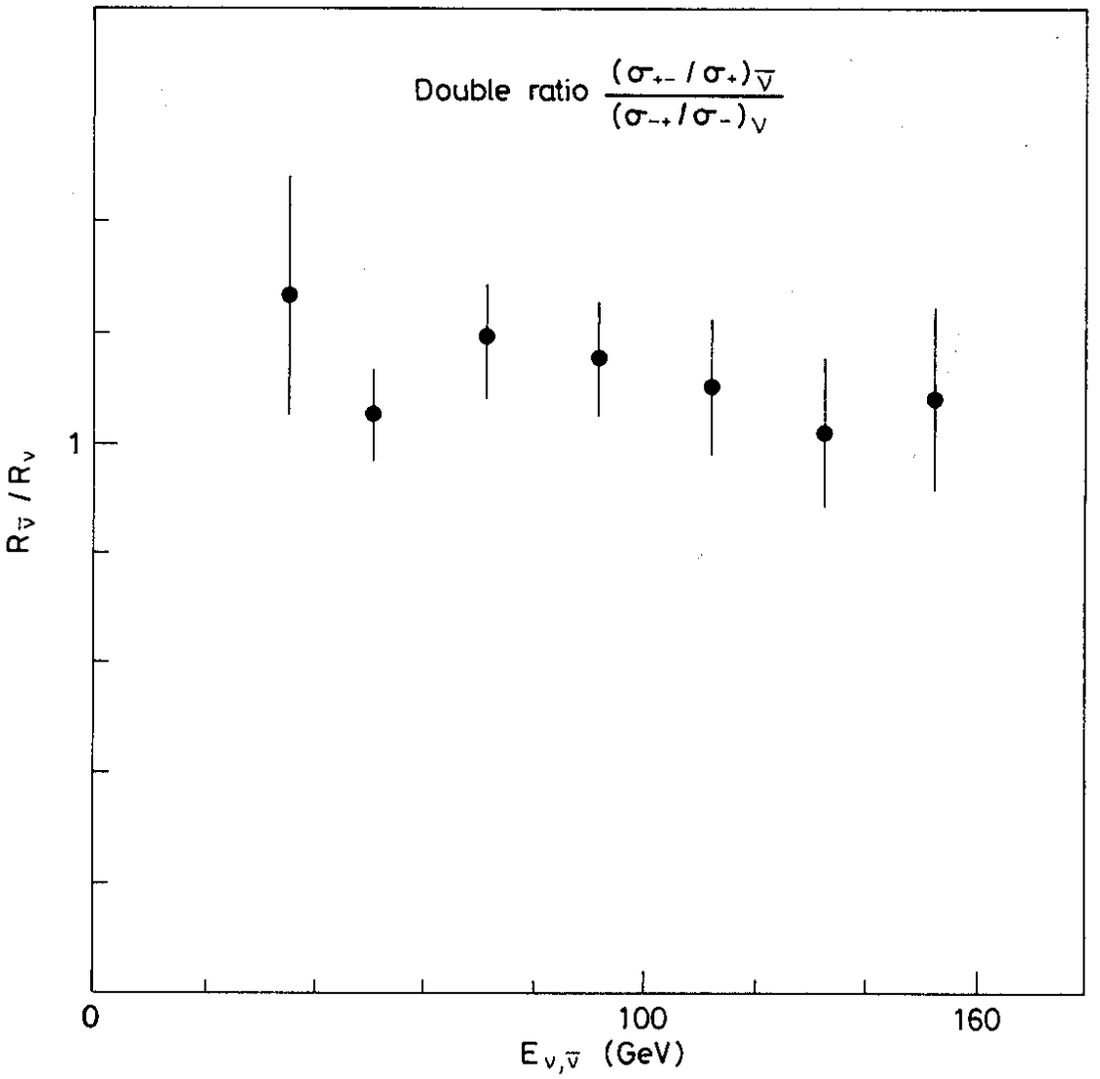
Double ratio $\frac{(\sigma_{+-}/\sigma_{+})_{\bar{\nu}}}{(\sigma_{-+}/\sigma_{-})_{\nu}}$
$R_{\bar{\nu}}/R_{\nu}$
1
0
100
160
$E_{\nu,\bar{\nu}}$ (GeV)

Fig. 14

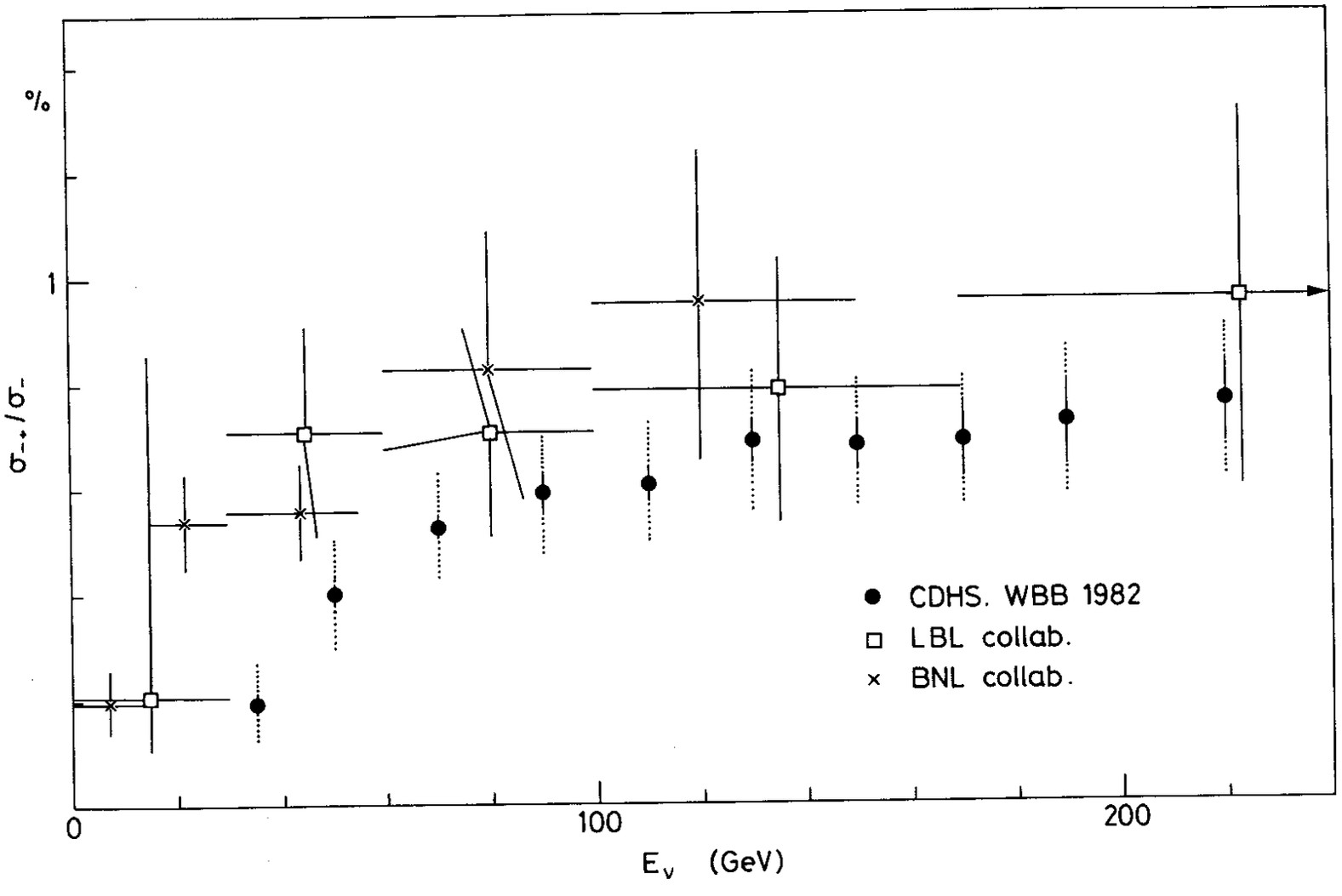
%
1
σ_{-+}/σ_{-}
0
100
200
E_ν (GeV)
CDHS. WBB 1982
LBL collab.
BNL collab.

Fig. 15

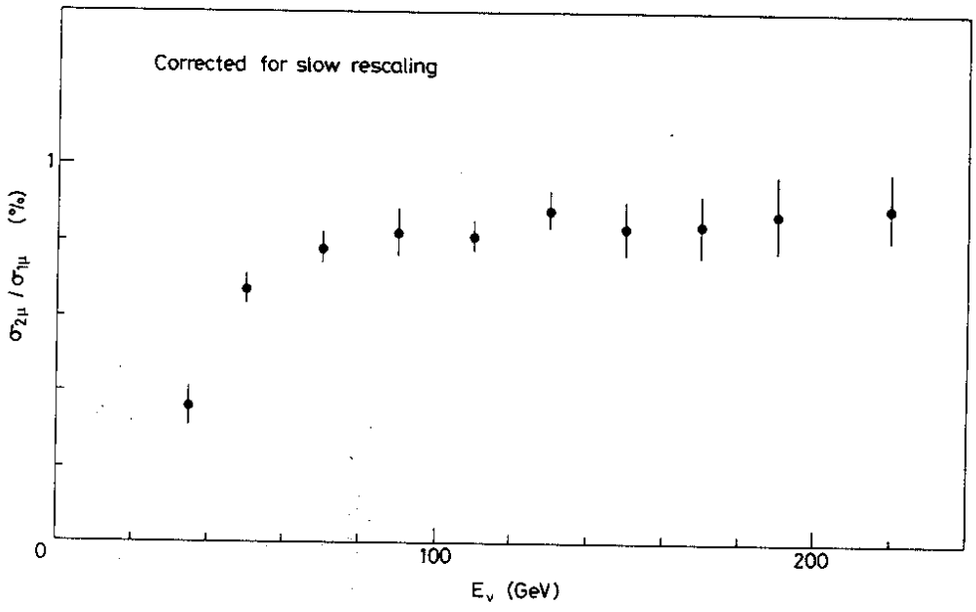
a)
Corrected for slow rescaling
1
0
100
200
E_ν (GeV)
$\sigma_{2\mu} / \sigma_{1\mu}$ (%)

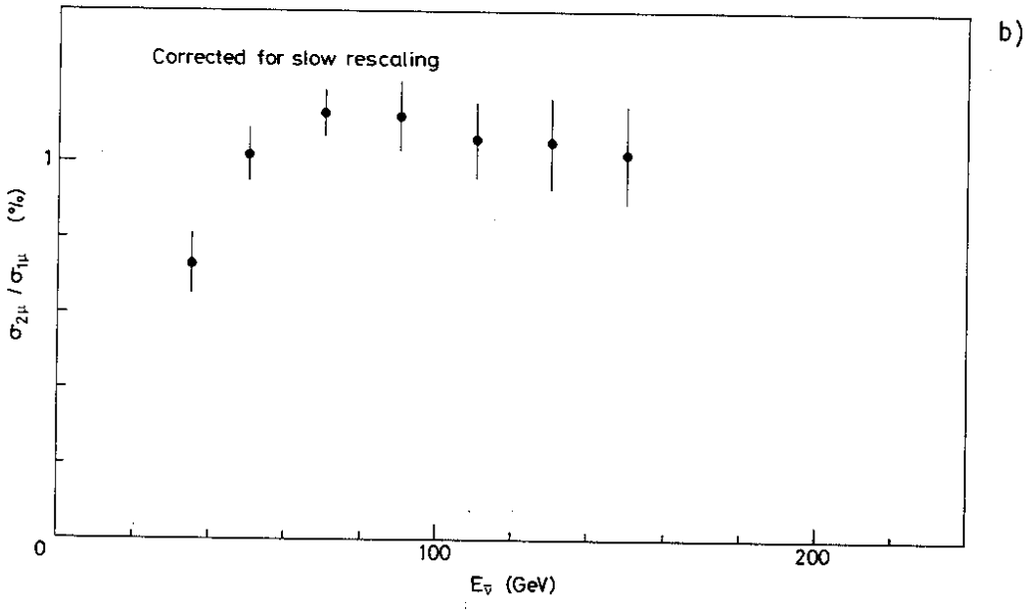
b)
Corrected for slow rescaling
1
0
100
200
$E_{\bar{\nu}}$ (GeV)
$\sigma_{2\mu} / \sigma_{1\mu}$ (%)

Fig. 16